Supporting Information

Unexpected Roles of Triethanolamine in the Photochemical Reduction of CO_2 to Formate by Ruthenium Complexes

Renato N. Sampaio,[†,*] David C. Grills,[†] Dmitry E. Polyansky,[†] David J. Szalda,[§] Etsuko Fujita[†,*]

[†]Chemistry Division, Brookhaven National Laboratory, Upton, NY 11973-5000, USA

[§]Department of Natural Science, Baruch College, CUNY, New York, NY 10010, USA

Table of Contents

1. *Supplementary UV-vis/ spectra of Ru(CO)(CO)$^{2+}$ monitoring its reactivity with TEOA and Hydroxide*

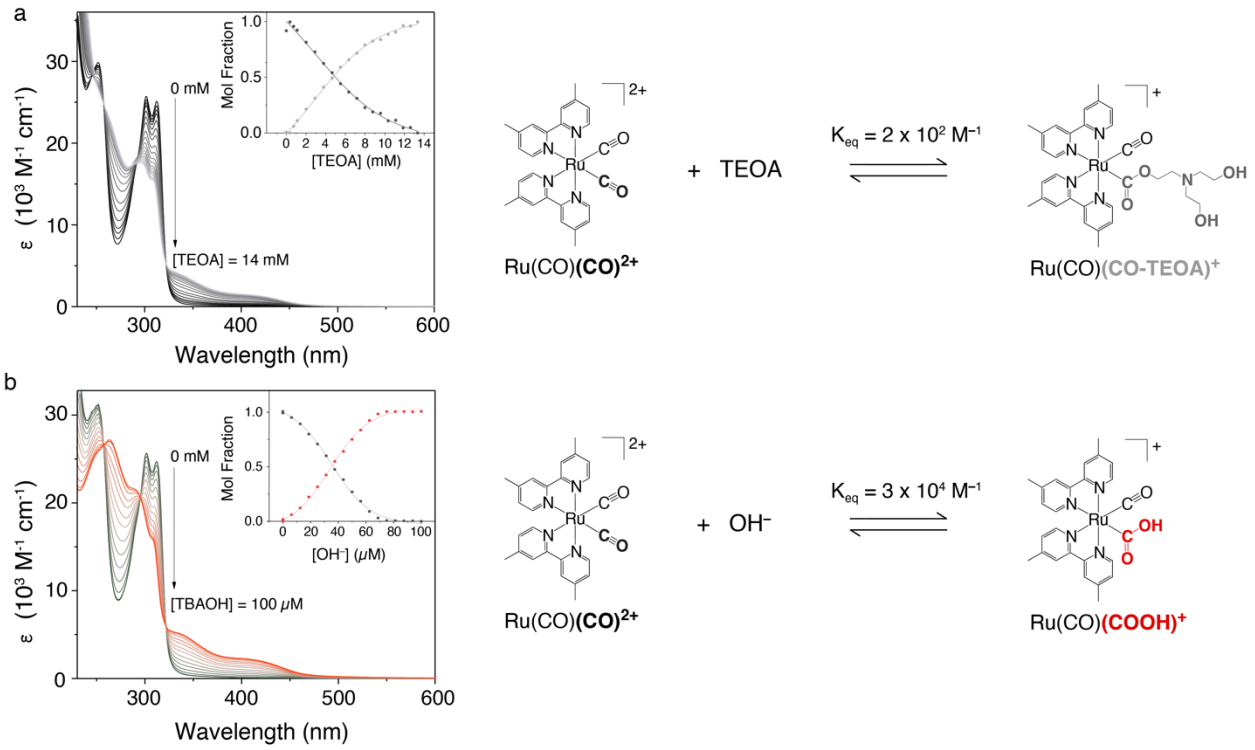

Figure S1. UV-vis spectral changes of Ru(CO)(CO)$^{2+}$ in acetonitrile solution upon titration of known concentrations of a) triethanolamine (TEOA) and b) TBAOH. Equilibrium constants were determined at the concentration of the respective added Lewis base when equal amounts of Ru(CO)(CO)$^{2+}$ and Ru(CO)(CO-TEOA)$^{+}$, or Ru(CO)(COOH)$^{+}$, existed. Note that in the case of the TEOA reaction, it is the deprotonated form of TEOA that binds to the complex.

2. *Supplementary IR spectra of Ru(CO)(CH₃CN)²⁺ monitoring its reactivity with TEOA*

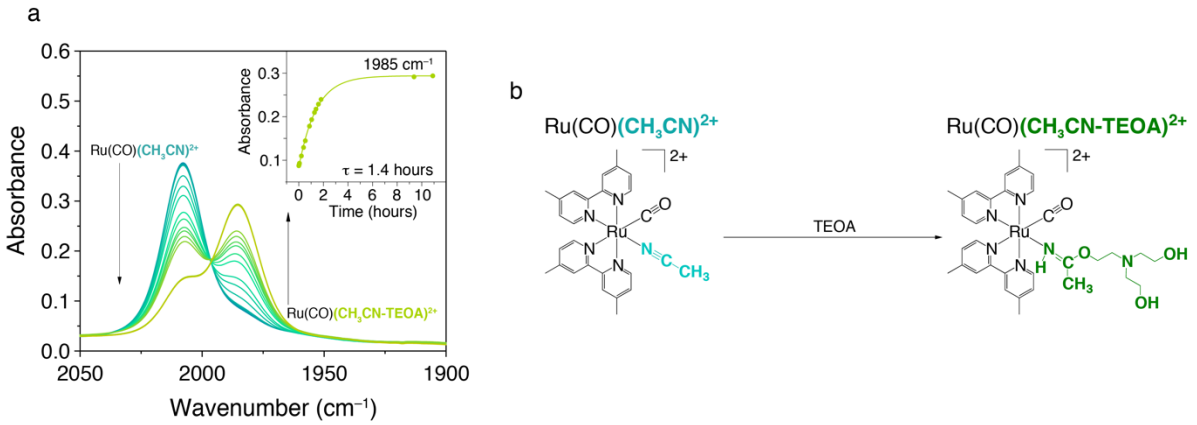

Figure S2. a) Mid-infrared absorption changes of the *ν*(CO) vibration of $Ru(CO)(CH_3CN)^{2+}$ monitored in 1.4 M TEOA/CH_3CN solution. b) Scheme depicting the reactivity of TEOA towards the $Ru(CO)(CH_3CN)^{2+}$ complex.

3. Supplementary crystallographic data for $Ru(CO)(CH_3CN)^{2+}$ and $Ru(CO)(CH_3CN\text{-}TEOA)^{2+}$

Determination and Refinement of the Structure. The structures were solved by using direct methods. In the least-squares refinement, anisotropic temperature parameters were used for all the non-hydrogen atoms except for the disordered acetone molecule in $[Ru(dmb)_2(CO)(CH_3CN)](PF_6)_2$ with occupancy factor of 0.3. The hydrogen atoms on the acetone molecule were not included in the final refinement. Hydrogen atoms were placed at calculated positions and allowed to "ride" on the atom to which they were attached except for the hydrogen atoms on the oxygen atoms of triethanolamine which were located on a difference Fourier map and included with fixed positional parameters. The isotropic thermal parameters for the hydrogen atoms were determined from the atom to which they are attached. The data were corrected for absorption using the multi-scan method (SADABS).

$Ru(dmb)_2(CO)(CH_3CN)](PF_6)_2$ consists of a Ru(II) center coordinated to two 4,4'-dimethyl-2,2'-bipyridyl ligands cis to one another and a carbonyl ligand with the acetonitrile ligand occupying the sixth coordination position. In *$[Ru(dmb)_2(CO)\{NHC(CH_3)\text{-}OC_2H_4\}N(C_2H_4OH)_2](PF_6)_2$* the sixth coordination site is occupied by the $NHC(CH_3)\text{-}OC_2H_4\}N(C_2H_4OH)_2$ ligand. Details of the crystallographic data collection and the refinement of the structures are presented in Table S1. Table S2 contains the bond lengths and angles in the coordination sphere for the two structures. The bond length between the Ru-atom and the nitrogen atom of the sixth ligand is slightly longer (0.028(4)Å) for the $NHC(CH_3)\text{-}OC_2H_4\}N(C_2H_4OH)_2$ ligand.

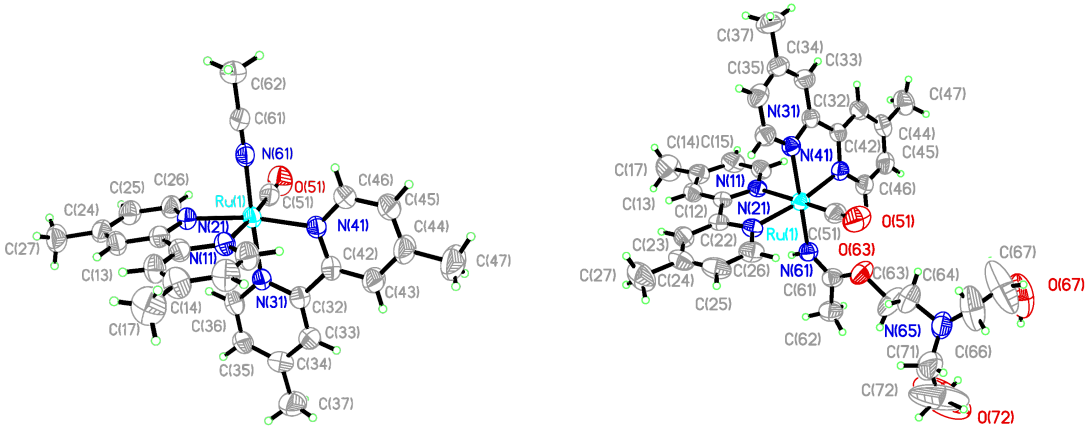

ORTEP drawings of *$Ru(dmb)_2(CO)(CH_3CN)]^{2+}$* (left) and *$[Ru(dmb)_2(CO)\{NHC(CH_3)\text{-}OC_2H_4\}N(C_2H_4OH)_2]^{2+}$* (right) cations.

The dihedral angle between the two dmb ligands is smaller in $[Ru(dmb)_2(CO)\{NHC(CH_3)\text{-}OC_2H_4\}N(C_2H_4OH)_2](PF_6)_2$ due to the larger size of the sixth ligand. Details of the hydrogen bonding in $[Ru(dmb)_2(CO)\{NHC(CH_3)\text{-}OC_2H_4\}N(C_2H_4OH)_2](PF_6)_2$ are shown in Table S3. The -OH groups at the end of the $\{NHC(CH_3)\text{-}OC_2H_4\}N(C_2H_4OH)_2$ ligand form hydrogen bonds with the -OH groups on a symmetry-related molecule. The ligand is somewhat disordered as it stretches away from the coordinated nitrogen because of the long flexible chain which contains both the donor groups and the accepting groups for the hydrogen bonds.

Table S1. Crystallographic Collection and Refinement Data for $[Ru(dmb)_2(CO)(CH_3CN)](PF_6)_2$ and $[Ru(dmb)_2(CO)\{NHC(CH_3)\text{-}OC_2H_4\}N(C_2H_4OH)_2](PF_6)_2$

	$[Ru(dmb)_2(CO)(CH_3CN)](PF_6)_2$	$[Ru(dmb)_2(CO)\{NHC(CH_3)\text{-}OC_2H_4\}N(C_2H_4OH)_2](PF_6)_2$
Formula	$C_{33}H_{39}O_3N_5P_2F_{12}Ru$	$C_{36}H_{48}O_5N_6P_2F_{12}Ru$
fw	944.70	1035.81
temp	296(2) K	296(2) K
cryst. syst.	Triclinic	Triclinic
space group	$P\bar{1}$	$P\bar{1}$
a (Å)	10.1169(7)	10.2665(4)
b (Å)	10.8235(7)	15.0186(5)
c (Å)	19.7200(13)	15.1586(6)
α (deg)	96.808(4)	106.802(2)
β (deg)	98.601(4)	98.455(2)
γ (deg)	101.702(3)	94.384(2)
V (Å^3)	2065.8(2)	2195.65(14)
Z	2	2
μ	0.550 mm^{-1}	0.529 mm^{-1}
λ (Å)	0.71073	0.71073
ρ calc (g cm^{-3})	1.519	1.567
cryst. size (mm)	0.43 × 0.33 × 0.10	0.43 × 0.33 × 0.10
θ range (deg)	2.07 to 26.00	1.68 to 27.50
total no. of reflns	50180	82354
no. of independent reflns, I ≥ 3.0σ(I)	7965 [R(int) = 0.1121] 5334	9998 [R(int) = 0.0828] 6288
no. of parameters	512	649
Final R indices [I>3.0σ(I)]	R1 = 0.0550, wR2 = 0.1439	R1 = 0.0498, wR2 = 0.1105
R indices (all data)	R1 = 0.0990, wR2 = 0.0828	R1 = 0.1058, wR2 = 0.1253
Goodness-of-fit on F2	0.981	0.998
Absorption correction	Semi-empirical from equivalents	Semi-empirical from equivalents

$R1 = \sum\big||F_o| - |F_c|\big| / \sum|F_o|$; $wR2 = \{\sum[w(|F_o^2| - |F_c^2|)^2] / \sum[w|F_o^2|^2]\}^{1/2}$

Table S2. Comparison of select bond lengths (Å) and angles (˚) in the coordination sphere of $[Ru(dmb)_2(CO)(NCCH_3)](PF_6)_2$ and $[Ru(dmb)_2(CO)\{NHC(CH_3)\text{-}OC_2H_4\}N(C_2H_4OH)_2](PF_6)_2$.

X =	$NCCH_3$	$\{N(H)C(CH_3)\text{-}OC_2H_4\}N(C_2H_4OH)_2$
Ru(1)-N(11)	2.101(4)	2.130(2)
Ru(1)-N(21)	2.071(4)	2.068(3)
Ru(1)-N(31)	2.052(3)	2.068(3)
Ru(1)-N(41)	2.066(4)	2.063(3)
Ru(1)-C(51)	1.849(5)	1.839(4)
Ru(1)-X	2.048(4)	2.076(3)
N(21)-Ru(1)-N(11)	77.85(14)	77.47(10)
N(31)-Ru(1)-N(11)	87.32(13)	85.32(10)
N(41)-Ru(1)-N(11)	93.99(14)	93.33(10)
C(51)-Ru(1)-N(11)	174.92(17)	172.85(14)
X -Ru(1)-N(11)	89.04(14)	88.35(10)
N(31)-Ru(1)-N(21)	93.86(14)	97.19(11)
N(41)-Ru(1)-N(21)	169.56(14)	170.19(10)
C(51)-Ru(1)-N(21)	97.15(17)	96.59(14)
X-Ru(1)-N(21)	89.56(14)	86.31(11)
N(41)-Ru(1)-N(31)	79.11(14)	78.46(11)
C(51)-Ru(1)-N(31)	93.95(17)	91.56(13)
X-Ru(1)-N(31)	174.37(14)	171.92(10)
C(51)-Ru(1)-N(41)	91.08(17)	92.34(14)
X-Ru(1)-N(41)	96.88(14)	96.93(11)
X-Ru(1)-N(51)	90.06(18)	95.29(13)
dmb-dmb	82.09(8)	76.29(5)

Table S3. Hydrogen bonds H···A (Å) and angles (deg) in $[Ru(dmb)_2(CO)\{NHC(CH_3)\text{-}OC_2H_4\}N(C_2H_4OH)_2](PF_6)_2$

D-H	d(D-H)	d(H..A)	<DHA	d(D..A)	A
N61-H61	0.860	2.171	173.97	3.028	F11 [-x+2, -y+1, -z+1]
N61-H61	0.860	2.429	151.61	3.211	F122 [-x+2, -y+1, -z+1]
O67-H67	1.115	1.735	132.52	2.621	O72 [-x+2, -y+3, -z+2]
O72-H72	0.868	2.012	177.77	2.880	O72 [-x+2, -y+3, -z+2]

4. Determination of equilibrium constant for the Zwitterionic capture of CO_2.

The equilibrium constant for the reaction described below was obtained via titration measurements of known amounts of CO_2 to a 0.7 M TEOA/CH_3CN solution while monitoring the mid-infrared absorption region characteristic of the C=O vibrations.

$$CO_2 + TEOA \rightleftharpoons CO_2TEOA$$

First, the molar absorption coefficient of free CO_2 was quantified in CH_3CN, Figure S3. Two syringe pumps with gas-tight syringes – one containing CO_2-saturated CH_3CN (0.28 M) and another with N_2-saturated CH_3CN – were used for the controllable mixing into an IR flow cell. The antisymmetric vibration of CO_2, 2342 cm^{-1}, was monitored as a function of the titrated amount of CO_2, from which the molar absorption coefficient was calculated (ε = 2039 M^{-1} cm^{-1}). At CO_2 concentrations > 20 mM, the IR absorption at 2342 cm^{-1} diverged from the predicted linear behavior of the Beer-Lambert law, and the IR absorption at 2330 cm^{-1} was used instead (ε = 345 M^{-1} cm^{-1}).

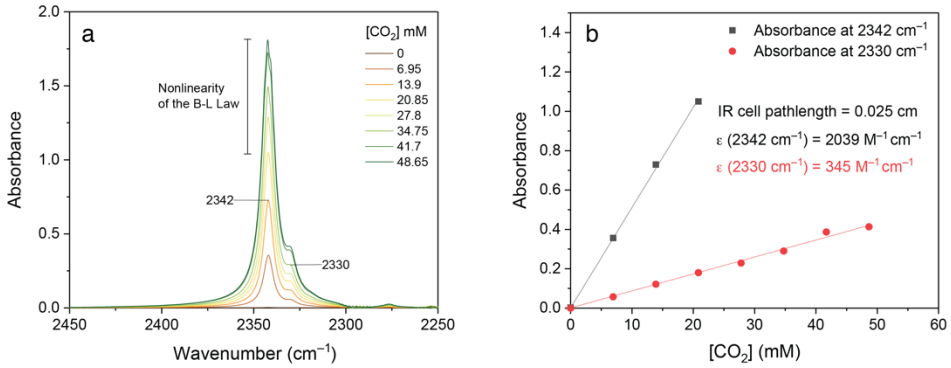

Figure S3. a) Mid-infrared absorption reporting on the *v*(CO) vibration of CO_2, at the indicated concentrations in CH_3CN. b) Plot of the concentration dependence of the absorbance, from which molar absorption coefficients at the indicated wavenumbers were obtained using the Beer-Lambert relationship. The spectral resolution of the FTIR spectrometer was set to 2 cm^{-1} for these measurements.

Knowing the molar absorption coefficient of CO_2 in CH_3CN allowed for quantification of its concentration via FTIR absorption measurements. The zwitterionic capture of CO_2 was monitored by using three syringe pumps containing: i) N_2-saturatured 1.4 M TEOA/CH_3CN, ii) N_2-saturated CH_3CN, and iii) CO_2-saturated CH_3CN solutions in gas-tight syringes. This configuration allowed for the titration of known amounts of free CO_2 into a 0.7 M TEOA/CH_3CN solution. The known concentration of added CO_2 was compared to that determined by the IR absorption at 2342 cm^{-1}

(or 2330 cm^{-1}) and the difference between them was assumed to be captured by TEOA to form the CO_2-TEOA zwitterion. Figure S4a compares the CO_2-TEOA concentration with the free CO_2 in solution, from which the slope provided a measure of the equilibrium constant, K_{eq} = 0.07 M^{-1}, according to,

$$K_{eq} = \frac{[CO_2 - TEOA]}{[CO_2^f][TEOA]} \quad ; \quad [CO_2 - TEOA] = K_{eq}[TEOA]\,[CO_2^f]$$

where the superscript *f* in $[CO_2^f]$ denotes the concentration of unreacted – or *free* – CO_2 that exists in the equilibrated mixture. The assumption that [TEOA] ≫ [CO_2-TEOA] was considered here.

The absorbance of the new IR band at 1646 cm^{-1} was plotted against the determined CO_2-TEOA concentration to obtain the molar absorption coefficient of the carbonyl asymmetric stretching band of the CO_2-TEOA zwitterion, Figure S4b (ε = 333 M^{-1} cm^{-1}).

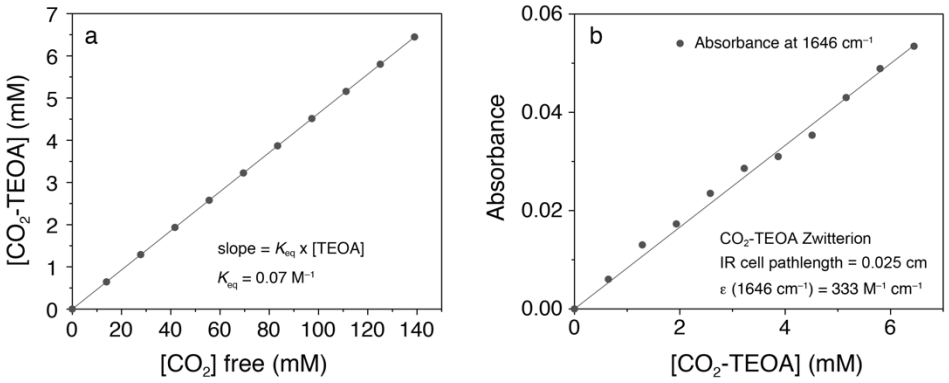

Figure S4. a) Plot of the calculated concentration of the zwitterionic CO_2-TEOA adduct as a function of the existing free CO_2 in the equilibrium mixture, from which the slope of the linear dependency provided an estimate for the equilibrium constant described in Figure 2c. b) Beer-Lambert plot of the CO_2-TEOA absorption peak measured at 1646 cm^{-1}. The spectral resolution of the FTIR spectrometer was set to 2 cm^{-1} for these measurements.

5. Supplementary cyclic voltammograms of $Ru(CO)(CH_3CN)^{2+}$ and $Ru(CO)(HCOO)^{+}$.

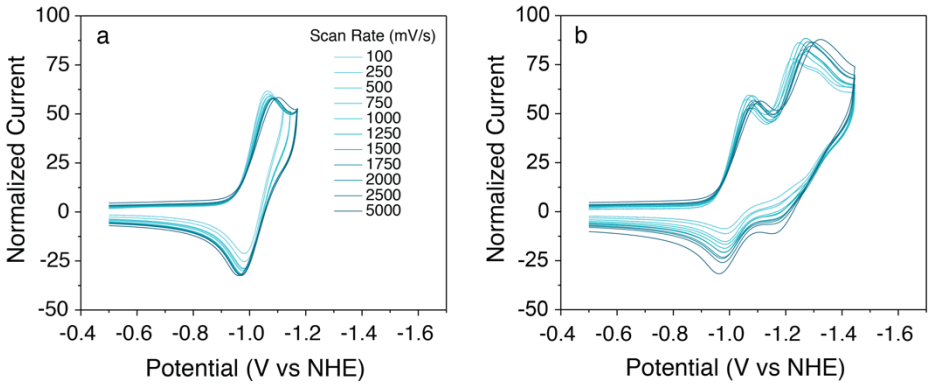

Figure S5. Cyclic voltammograms for a 1 mM solution of the $Ru(CO)(CH_3CN)^{2+}$ complex measured at the indicated scan rates, in 0.1 M $TBAPF_6$ anhydrous CH_3CN. Potentials were converted to NHE using $E_{1/2}(Fc^{+/0})$ = 0.63 V vs NHE in CH_3CN as the scaling factor.[1]

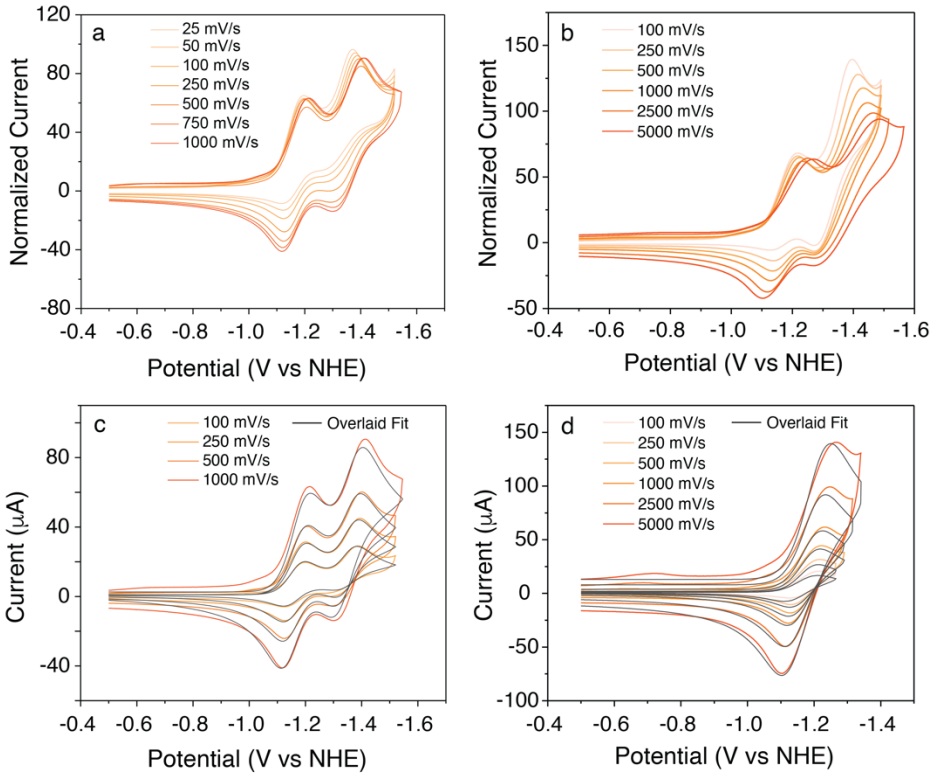

Figure S6. Cyclic voltammograms for a 1 mM solution of the $Ru(CO)(HCOO)^{+}$ complex measured at the indicated scan rates, in a) 0.1 M $TBAPF_6$ anhydrous CH_3CN and b) with added 50 mM TEOA. Shown in panels c) and d) are overlaid fits (black traces) of $Ru(CO)(HCOO)^{+}$ voltammogram data at the indicated scan rates in CH_3CN and 50 mM TEOA/CH_3CN respectively. Potentials were converted to NHE using $E_{1/2}(Fc^{+/0})$ = 0.63 V vs NHE in CH_3CN as the scaling factor.[1]

The equations used in the DigiSim simulation software to model the electrochemical data are listed in Table S4.

Table S4. Equations used in the DigiSim simulations shown in Figures S6c and S6d.

		CH_3CN	50 mM TEOA/CH_3CN
$Ru(CO)(HCOO)^+ + e^- \rightleftharpoons Ru(CO)(HCOO)^0$	1st electrochemical step	✓	✓
$Ru(CO)(HCOO)^0 \rightleftharpoons Ru(CO)^+ + HCOO^-$	1st chemical step	✓	✓
$Ru(CO)(HCOO)^0 + e^- \rightleftharpoons Ru(CO)(HCOO)^-$	3nd electrochemical step	✓	
$Ru(CO)(HCOO)^- \rightleftharpoons Ru(CO)^0 + HCOO^-$	2nd chemical step	✓	

Table S5 lists the equilibrium and kinetic parameters for formate dissociation from the singly- and doubly-reduced $Ru(CO)(HCOO)^+$ complex, obtained from the DigiSim simulations shown in Figures S6b and S6c. We should note that due to the large number of equations used in the simulations (Table S4), and thus the large number of fitting parameters, these values may be subject to large errors.

Table S5. Equilibrium and kinetic parameters for $HCOO^-$ dissociation.[a]

Reaction	$Ru(CO)(HCOO)^+$ Kinetic Parameters			
	CH_3CN		50 mM TEOA/CH_3CN	
	K_{eq} (M)	k_f (s^{-1})	K_{eq} (M)	k_f (s^{-1})
$Ru(CO)(HCOO)^0 \rightleftharpoons Ru(CO)^+ + HCOO^-$	0.03	0.07	3.9	1.0
$Ru(CO)(HCOO)^- \rightleftharpoons Ru(CO)^0 + HCOO^-$	430	0.66		

[a]Values were extracted from simulated scan-rate dependent cyclic voltammograms of the $Ru(CO)(HCOO)^+$ catalyst shown in Figure S6.

6. Na-Hg Reduction

Experimental Procedure for Na-Hg Reduction

Sodium amalgam (~0.5% Na in Hg) was prepared by dissolving sodium metal in mercury in a fume hood and storing under argon. Spectroscopic grade CH_3CN was dried over CaH_2, distilled, and degassed by carrying out freeze-thaw cycles using a high-vacuum line. After molecular sieves in a round bottom flask were activated at 300 °C overnight using a high-vacuum line, the purified CH_3CN was vacuum-transferred into the glassware containing the activated molecular sieves.

Home-made glassware equipped with an optical cell (1 – 10 mm pathlength), a Na-Hg chamber separated by a glass frit and a metal valve (or high-vacuum stopcock) was used for Na-Hg reduction experiments. The typical amount of metal complex used was much less than 1 mg, and an excess of Na-Hg was used. The glassware was placed on a high-vacuum line (~ 10^{-6} torr) and the CH_3CN mentioned above (2 – 4 mL) was vacuum-distilled into it. The glassware was then sealed and removed from the vacuum line. Stepwise Na-Hg reduction of the complex was performed under vacuum by moving a small amount of the solution to the Na-Hg chamber for a short time, and then back into the other chamber, followed by a UV-vis spectral measurement. The reduction process was gradually continued in this manner, with each step of the reduction resulting from the net transfer of one electron to the metal complex being determined by a loss of isosbestic points in the UV-vis spectra. This method has previously been used by our group for various systems.[2-7]

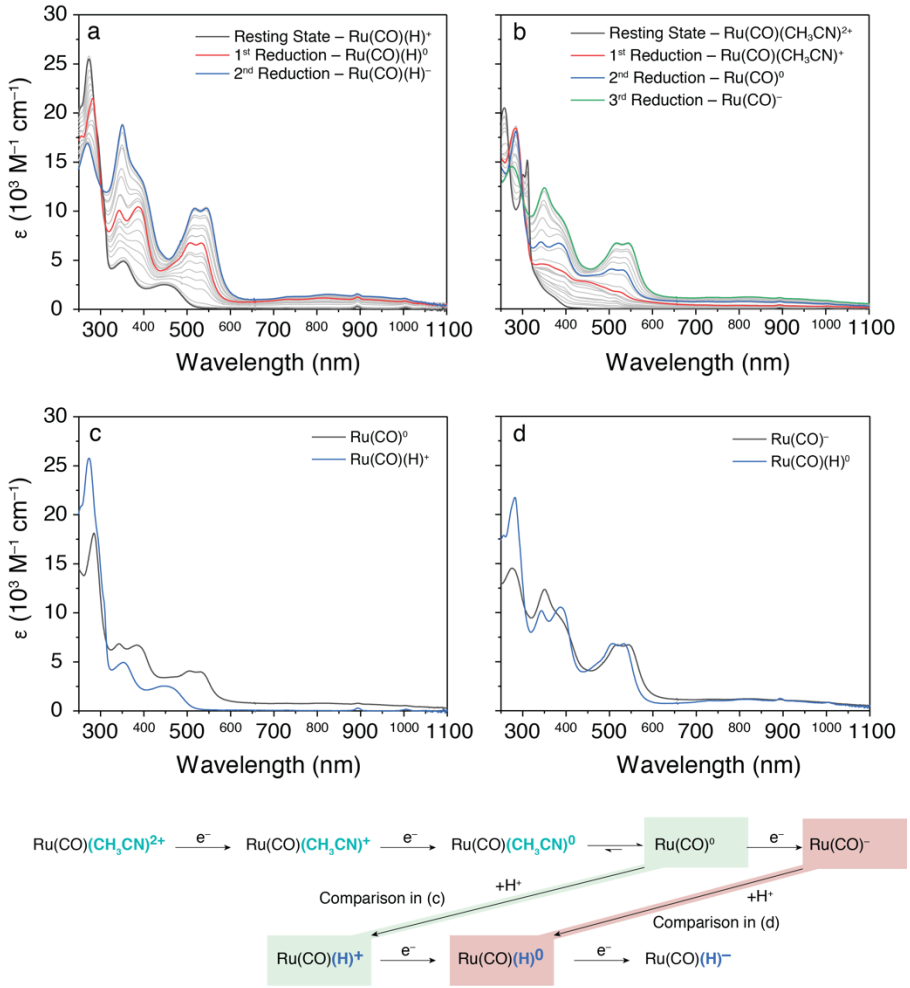

Figure S7. Sodium amalgam (Na-Hg) reduction of the (a) $Ru(CO)(H)^+$ and (b) $Ru(CO)(CH_3CN)^{2+}$ complexes in CH_3CN. c) Comparison of the UV-vis spectrum of $Ru(CO)(CH_3CN)^{2+}$ after being reduced by two electrons with the spectrum for $Ru(CO)(H)^+$. d) Comparison of the UV-vis spectrum of $Ru(CO)(CH_3CN)^{2+}$ after being reduced by three electrons with the spectrum for $Ru(CO)(H)^0$. The diagram at the bottom describes the expected redox states and chemical transformations for each complex. A list of the isosbestic points used to monitor each reduction step is provided below.

Reduction Step	Isosbestic Point (nm)
$Ru(CO)(H)^+ + e^- \rightarrow Ru(CO)(H)^0$	312
$Ru(CO)(H)^0 + e^- \rightarrow Ru(CO)(H)^-$	300
$Ru(CO)(CH_3CN)^{2+} + e^- \rightarrow Ru(CO)(CH_3CN)^+$	298 / 321
$Ru(CO)(CH_3CN)^+ + e^- \rightarrow Ru(CO)^0$	311
$Ru(CO)^0 + e^- \rightarrow Ru(CO)^-$	301

7. *Supplementary charge recombination kinetics from the singly-reduced Ru(CO)(X)$^{(n-1)+}$ complexes to BIH$^{\bullet+}$, in the absence of TEOA.*

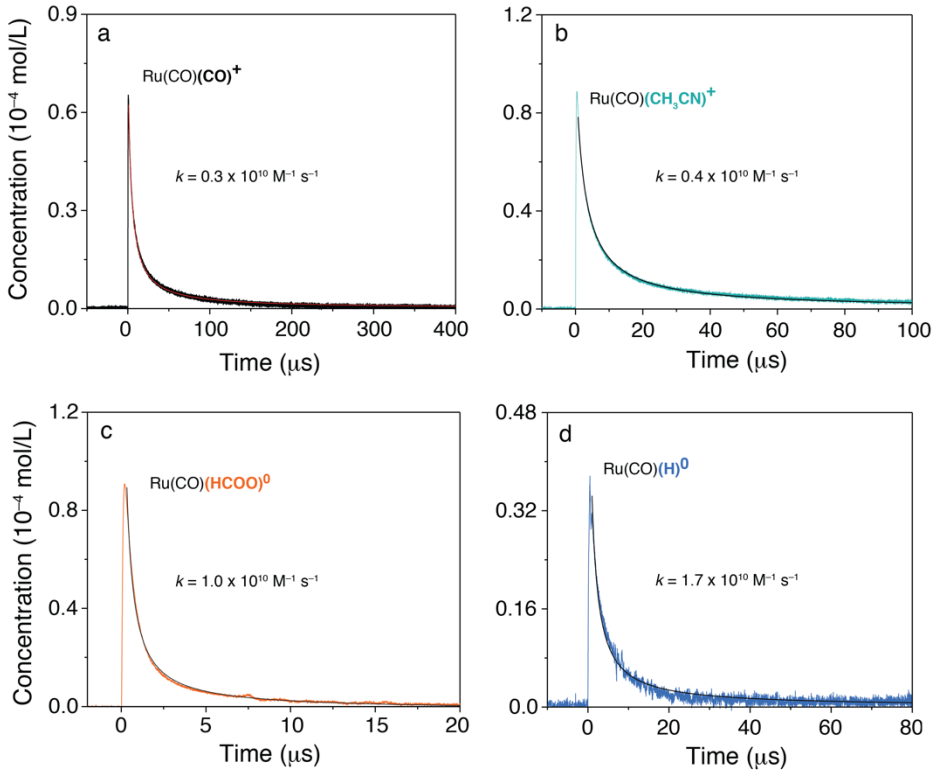

Figure S8. Time-dependent concentration traces of singly-reduced Ru(CO)(X)$^{(n-1)+}$ complexes measured at their corresponding *ν*(CO) peak, in N_2-saturated CH_3CN solutions containing 5 mM Ru(CO)(X)$^{n+}$, 0.5 mM $[Ru(bpy\text{-}OMe)_3]^{2+}$ and 0.2 M BIH. Overlaid in black are fits to a second order equal concentration kinetic function.

The spectral changes corresponding to each kinetic trace in Figure S8 can be found in:

Kinetic trace	Full transient spectra
Figure S8a	Figure 5a
Figure S8b	Figure S9a
Figure S8c	Figure 6a
Figure S8d	Figure 7a

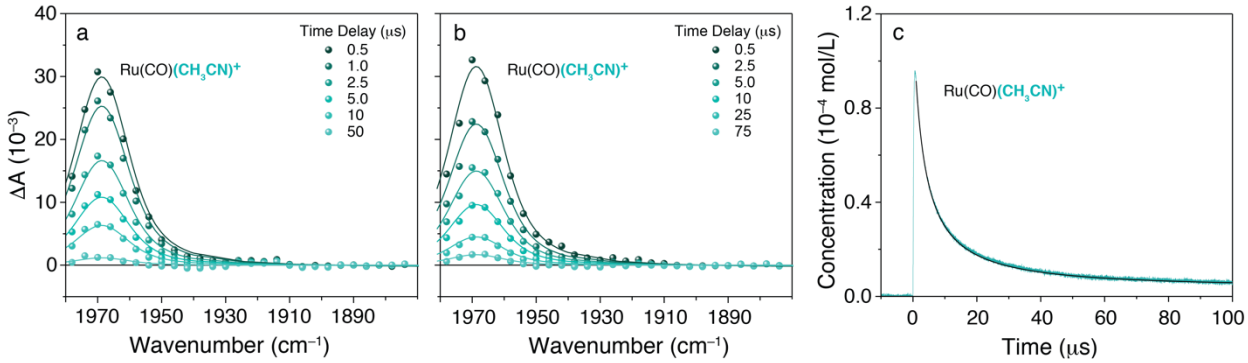

Figure S9. TRIR absorption changes of the $Ru(CO)(CH_3CN)^{2+}$ complex measured at the indicated time delays after pulsed 532 nm excitation of the $[Ru(bpy\text{-}OMe)_3]^{2+}$ chromophore: a) measured in neat CH_3CN solution and b) measured in 1.4 M TEOA/CH_3CN solution. Overlaid are spectral simulations based on a least squares fit of known ν(CO) IR spectra. c) Simulated time-dependent concentration profile of the transient species based on the least-squares fit global analysis. Note that data in the 2005 – 1980 cm^{-1} range are not available due to the available tuning ranges of our infrared laser probes.

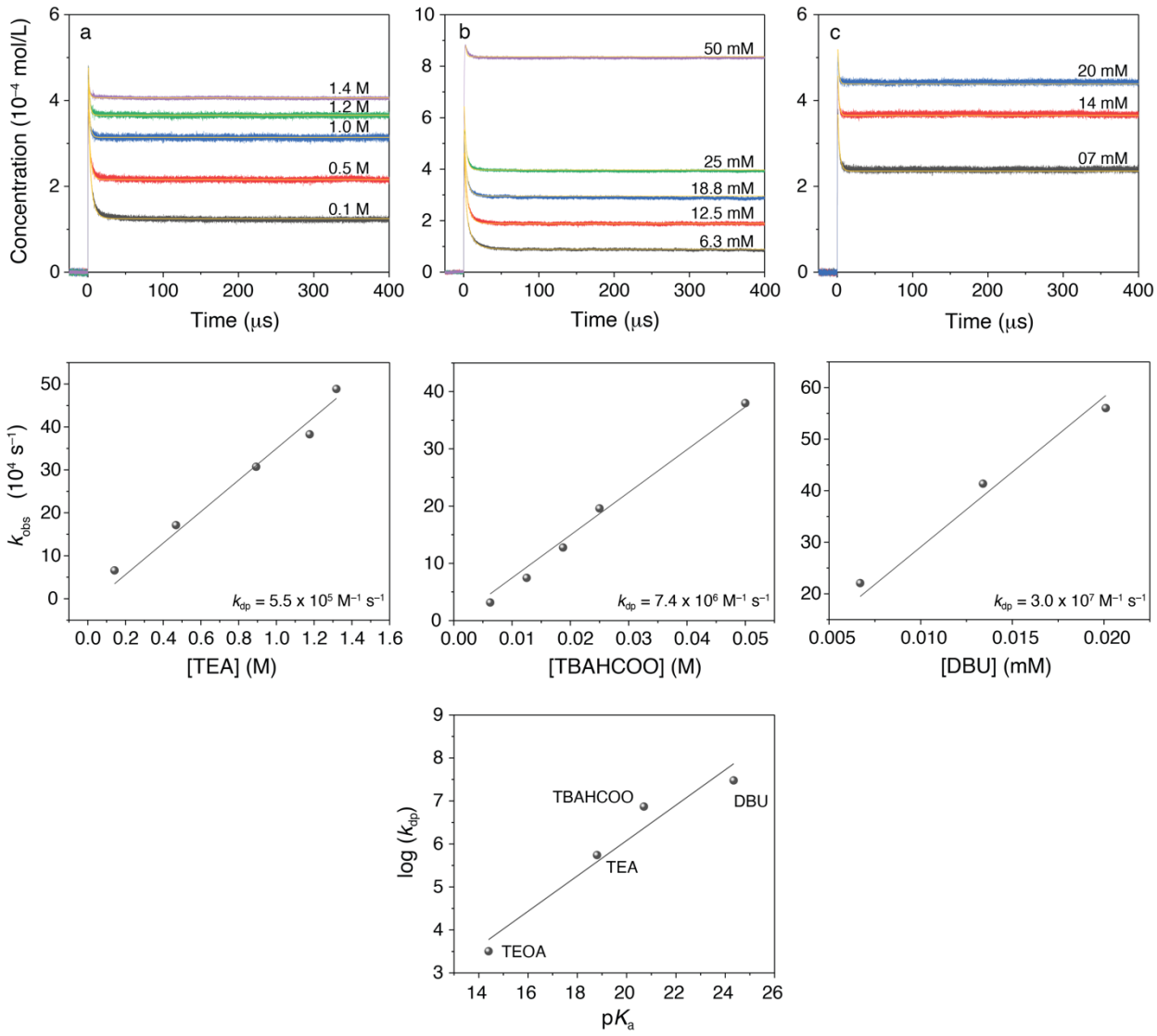

Figure S10. Kinetic traces measured at 1894 cm^{-1} that report on the concentration profile of the photochemically-generated, singly-reduced $Ru(CO)(H)^0$ complex. Experiments were performed by varying the titrated amount of supporting base, a) TEA, b) $TBAHCOO^-$, and c) DBU. Overlaid in yellow are fits to the numerical solution of equations 1 and 2 described in the main text. The graphs that follow in the bottom panel are representative of the observed rate constants for deprotonation of $BIH^{\bullet+}$ as a function of the concentration of added base, from which the second-order rate constants were calculated. The graph shown at the bottom of Figure S10 relates the logarithm of the measured k_{dp} with the corresponding pK_a of the conjugate acid of the added Brønsted base.

8. Supplementary TRIR data for Ru(CO)(CO-TEOA)$^+$, Ru(CO)(HCOO)$^+$ and Ru(CO)(H)$^+$.

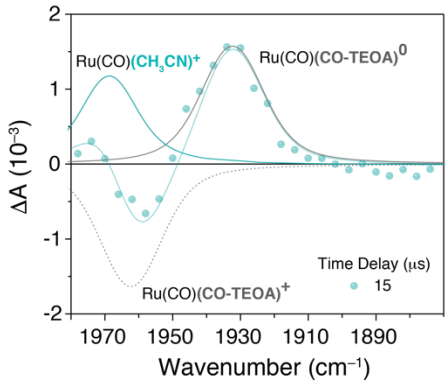

Figure S11. Representative least squares global fit analysis of the Ru(CO)(CO-TEOA)$^+$ TRIR data taken at 15 μs after pulsed 532 nm excitation of the $[Ru(bpy\text{-}OMe)_3]^{2+}$ chromophore in 1.4 M TEOA/CH_3CN, N_2-saturated solution. The reference spectra of the *bleached* Ru(CO)(CO-TEOA)$^+$, Ru(CO)(CO-TEOA)^0 and Ru(CO)(CH_3CN)$^+$ were included to satisfactorily model the transient data.

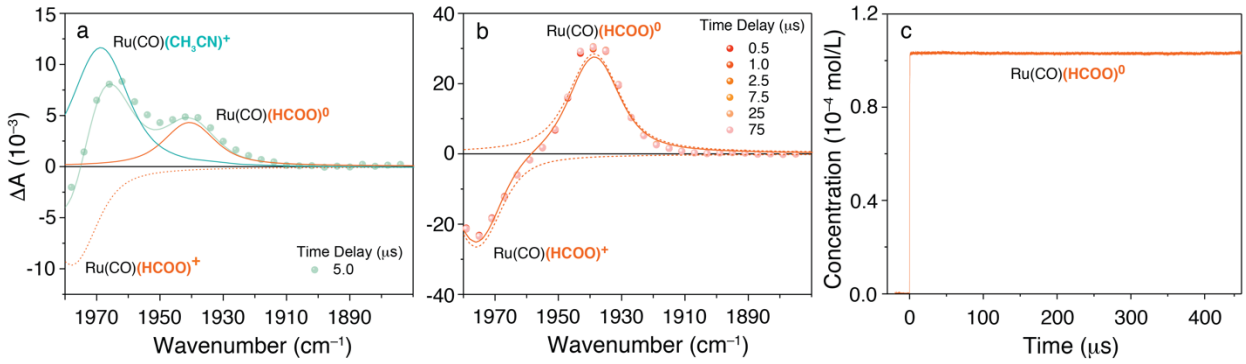

Figure S12. a) Representative least squares global fit analysis of the Ru(CO)(HCOO)$^+$ TRIR data taken at 5 μs after pulsed 532 nm excitation of the $[Ru(bpy\text{-}OMe)_3]^{2+}$ chromophore in 1.4 M TEOA/CH_3CN, N_2-saturated solution. The reference spectra of the *bleached* Ru(CO)(HCOO)$^+$, Ru(CO)(HCOO)^0 and Ru(CO)(CH_3CN)$^+$ were included to satisfactorily model the transient data. b) TRIR absorption changes of the Ru(CO)(HCOO)$^+$ complex at the indicated time delays after pulsed 532 nm excitation of the $[Ru(bpy\text{-}OMe)_3]^{2+}$ chromophore in 50 mM TBAHCOO/CH_3CN solution. Overlaid are spectral simulations based on a least squares fit of the indicated known ν(CO) IR spectra. c) Simulated time-dependent concentration profile of the singly-reduced Ru(CO)(HCOO)^0 based on the least-squares fit global analysis.

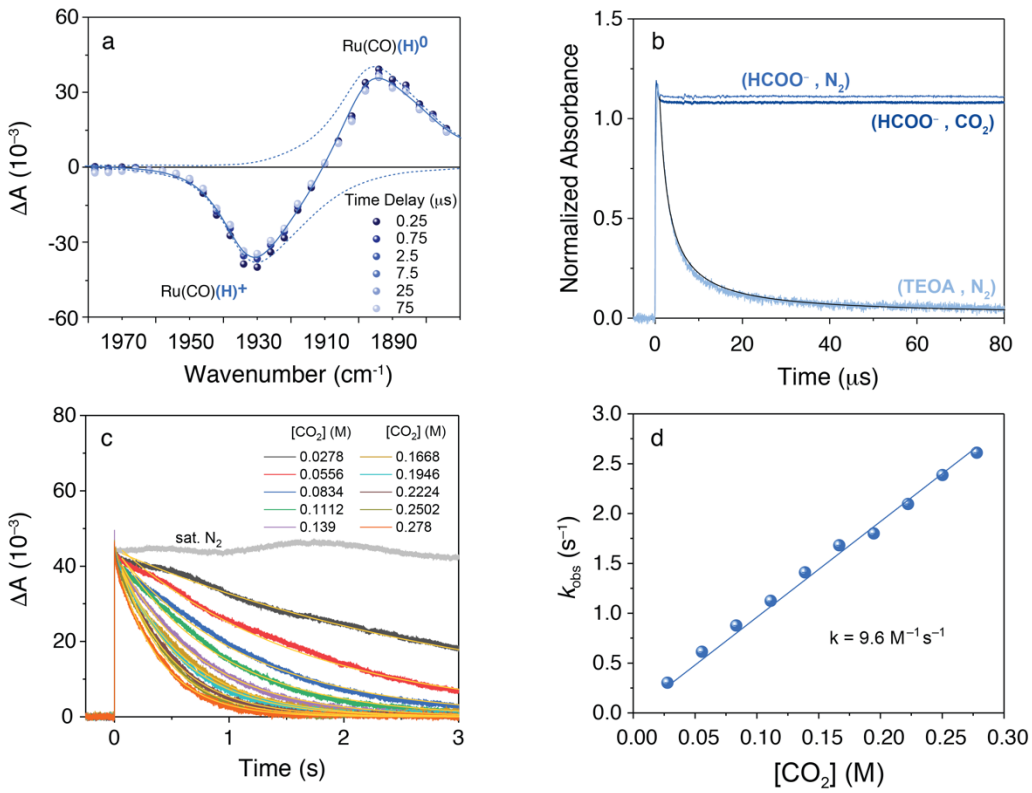

Figure S13. a) TRIR absorption changes of the $Ru(CO)(H)^+$ complex at the indicated time delays after pulsed 532 nm excitation of the $[Ru(bpy\text{-}OMe)_3]^{2+}$ chromophore in 50 mM $TBAHCOO/CH_3CN$, N_2-saturated solution. Overlaid are spectral simulations based on a least squares fit of the data with the known IR spectra for $Ru(CO)(H)^+$ and $Ru(CO)(H)^0$. b) Normalized kinetic traces at 1894 cm^{-1}, measured in 50 mM $TBAHCOO/CH_3CN$ N_2-saturated solution, 50 mM $TBAHCOO/CH_3CN$ CO_2-saturated solution, or 1.4 M $TEOA/CH_3CN$ N_2-saturated solution. c) Transient absorption changes indicative of the hydride transfer step to CO_2 measured at the $Ru(CO)(H)^0$ peak, 1894 cm^{-1}, for the indicated concentrations of CO_2 in 50 mM $TBAHCOO/CH_3CN$ solutions. d) Plot of the observed rates of decay from panel c as a function of the CO_2 concentration, from which the second-order rate constant for hydride transfer to CO_2 was obtained.

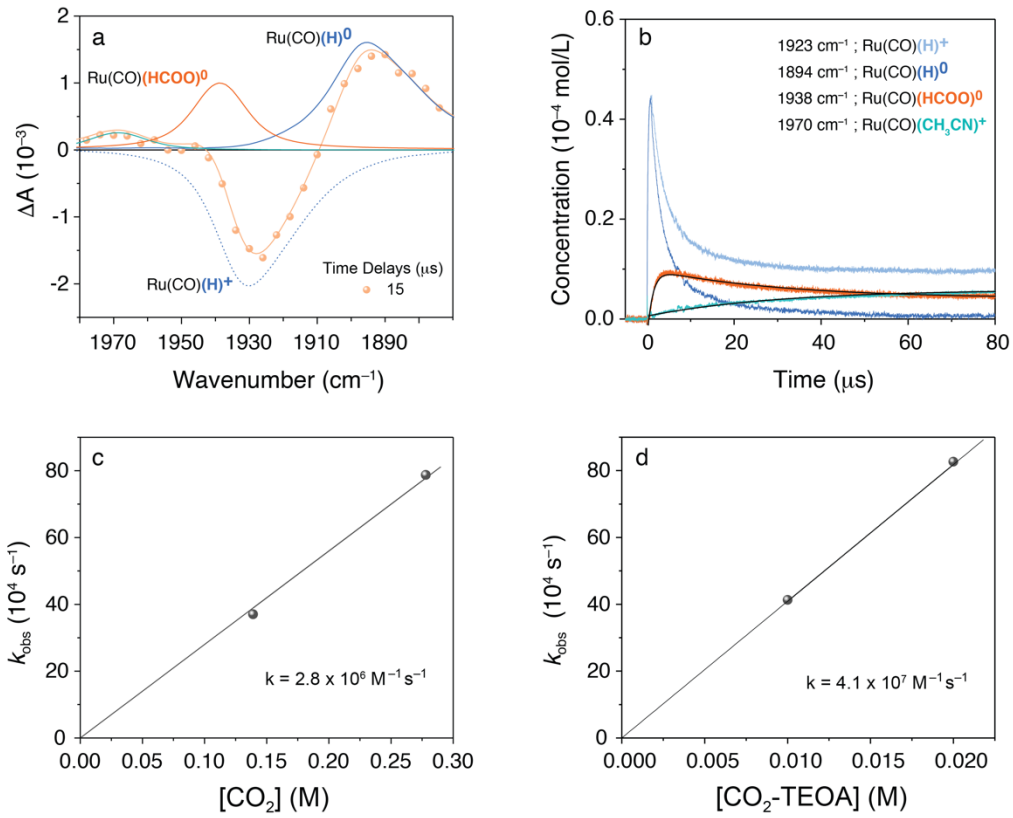

Figure S14. a) Representative least squares global fit analysis of the data in Figure 7b taken at 15 μs after pulsed 532 nm excitation. The reference spectra of the *bleached* $Ru(CO)(H)^+$, $Ru(CO)(H)^0$, $Ru(CO)(HCOO)^0$ and $Ru(CO)(CH_3CN)^+$ were included to satisfactorily model the transient data. b) Single kinetic traces measured at wavenumbers that corresponded to absorption changes predominant of the indicated transient species (the data were converted to concentration profiles using the known molar absorption coefficients of each species and the cell pathlength); the raw kinetic trace representative of $Ru(CO)(HCOO)^0$ at 1938 cm^{-1} was subtracted by the contribution of *bleached* $Ru(CO)(H)^+$. Plots of the observed rates for the formation of $Ru(CO)(HCOO)^0$ as a function of (c) the CO_2 concentration, and (d) the CO_2-TEOA concentration, from which the second-order rate constants for hydride transfer to CO_2 and CO_2-TEOA, were obtained, respectively.

9. *Hydricity determination and thermodynamic relationships used for the calculation of hydricity and pK_a of the metal hydrides in acetonitrile solutions.*

The hydricity value for $[Ru(dmb)_2(CO)(H)]^+$ was determined experimentally using the direct hydride transfer method relative to $[Ru(HMB)(bpy)(H)]^+$ (ΔG_{H^-} = 54 ± 2 kcal mol^{-1})[8] as the reference hydride, and relative to the hydricity of H_2 by stoichiometric addition of protonated triethylamine,[9] $TEAH^+$ (pK_a = 18.82)[10-11], as the proton source.

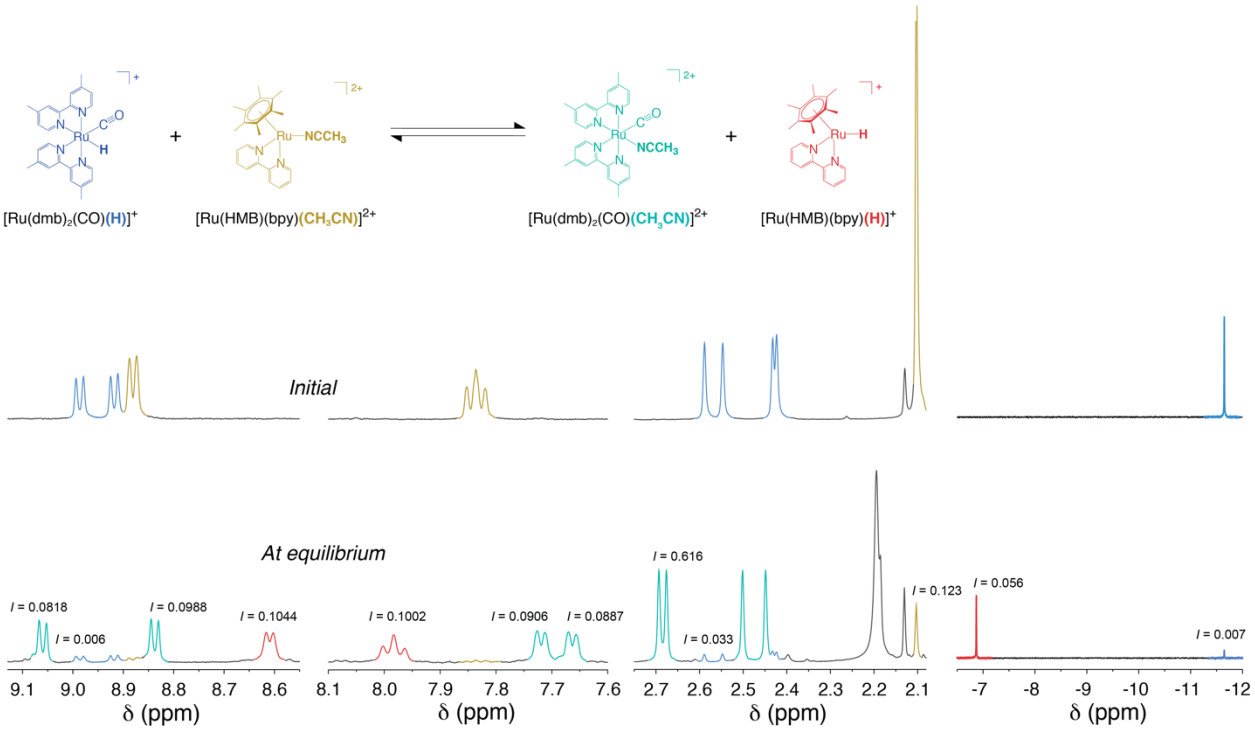

Figure S15. ^{1}H-NMR spectra of the reaction equilibrium illustrated in the figure in CD_3CN solution. The metal hydrides, $[Ru(dmb)_2(CO)(H)]^+$ and $[Ru(HMB)(bpy)(CH_3CN)]^{2+}$ were mixed at near equimolar quantities for six independent experiments, from which the obtained equilibrium constants were used to calculate an average hydricity value.

Figure S15 shows the ^{1}H-NMR spectra of the solution mixture ($[Ru(dmb)_2(CO)(H)]^+$: $[Ru(HMB)(bpy)(CH_3CN)]^{2+}$ in CD_3CN) at near equimolar concentration before and after the reaction has achieved equilibrium. The solution mixture was heated to 80^o C for multiple intervals of 10 minutes and the reaction equilibrium was monitored by ^{1}H-NMR at 25^o C. Equilibrium was established after 1 hour of accumulated heating. The indicated integral values were used to

quantify the equilibrium constants, from which a hydricity value for $[Ru(dmb)_2(CO)(H)]^+$ of ΔG_{H^-} = 51 ± 0.5 kcal mol^{-1} was obtained relative to $[Ru(HMB)(bpy)(H)]^+$ (ΔG_{H^-} = 54 ± 2 kcal mol^{-1}) using equation S1. The obtained value was averaged over six independent experiments at similar conditions.

$$\Delta G_{H^-} = \Delta G_{H^-}(ref.) - 1.364 \log(K_{eq}) \quad \text{S1}$$

In a separate experiment, $[Ru(dmb)_2(CO)(H)]^+$ and $TEAH^+$ were mixed in a 1:10 concentration ratio in CD_3CN and added to an air-free NMR tube. Equilibrium was monitored at multiple intervals of 10 minutes of heating at 80° C. Equilibrium was achieved after 1 hour. The hydricity of $[Ru(dmb)_2(CO)(H)]^+$ was determined by measuring the equilibrium constant for,

$$[Ru(dmb)_2(CO)(H)]^+ + TEAH^+ \rightleftharpoons [Ru(dmb)_2(CO)(CH_3CN)]^{2+} + TEA + H_2$$

according to equation S2,

$$\Delta G_{H^-} = -1.364 \times \log(K_{eq}) - 1.364 \times pK_a(TEAH^+) + 77 \quad \text{S2}$$

Integration of the NMR data for $[Ru(dmb)_2(CO)(H)]^+$ and $[Ru(dmb)_2(CO)(CH_3CN)]^{2+}$ provided K_{eq} = 3.68 atm (the amount of $TEAH^+$ converted to TEA was assumed to be equal to the amount of $[Ru(dmb)_2(CO)(H)]^+$ that has been converted to $[Ru(dmb)_2(CO)(CH_3CN)]^{2+}$; similarly, the partial pressure of H_2 was calculated by assuming that the amount of H_2 produced was equal to $[Ru(dmb)_2(CO)(CH_3CN)]^{2+}$). The hydricity obtained by this method for $[Ru(dmb)_2(CO)(H)]^+$, ΔG_{H^-} = 50.6 kcal mol^{-1}, is in good agreement with the value determined using the direct hydride transfer method.

The final hydricity for $[Ru(dmb)_2(CO)(H)]^+$, ΔG_{H^-} = 51 ± 0.5 kcal mol^{-1}, was obtained by averaging the values from the two experimental methods discussed above.

Complementary DFT calculations were also conducted to estimate the hydricity value of $[Ru(dmb)_2(CO)(H)]^+$ using an isodesmic relationship with $[Ru(tpy)(bpy)(H)]^+$ as the reference metal hydride (ΔG_{H^-} = 39 ± 3 kcal mol^{-1}).[5, 12] We note here that the original work from Creutz and co-authors experimentally determined the hydricity of $[Ru(tpy)(bpy)(H)]^+$ as ΔG_{H^-} = 39 ± 3 kcal mol^{-1},[5] while a review article from Appel, Miller and co-authors on hydricity of metal hydrides mistakenly cited this value with too high a precision,[8] 39.3 kcal mol^{-1}. The reaction free energy change for a hydride transfer between $Ru(tpy)(bpy)(H)^+$ and $Ru(CO)(CH_3CN)^{2+}$,

$Ru(tpy)(bpy)H^+ + Ru(CO)(CH_3CN)^{2+} \rightleftharpoons Ru(tpy)(bpy)(CH_3CN)^{2+} + Ru(CO)(H)^+$ ($\Delta G^\circ = -11.5$ kcal/mol^{-1}) S3

was computationally determined by comparing the total free energies of each optimized structure. This value was then added to the hydricity of the reference compound, $[Ru(tpy)(bpy)(H)]^+$. In using this approach, errors inherent to the computational methods are thought to be minimized since they are *cancelled out* by taking the difference in free energy. The computed free energy for the reaction equilibrium described in equation S3 was $\Delta G^\circ = -11.5$ kcal mol^{-1} exergonic, and therefore provided a calculated hydricity for $[Ru(dmb)_2(CO)(H)]^+$ of $\Delta G_{H^-} = 50.8$ kcal mol^{-1}.

For all other hydricity values – *at different redox states of the metal hydride* – as well as the acidity ($\Delta G_{H^+} = 1.364 \times pK_a$) and the homolytic M–H bond cleavage ($\Delta G_{H^\bullet}$), thermochemical cycles were used by relating these quantities to reduction potentials ($E_{1/2}$) through free energy relationships.[8] The diagram below exemplifies this combination of free energies for a cationic metal hydride $[M–H]^+$ – in its resting state – and its hypothetically accessible redox states, with those of the parent complex which considers a solvent molecule coordinated to the metal. Note that the diagram below omits the signs (*positive* or *negative*) that accompany each thermodynamic quantity for a specific reaction path.

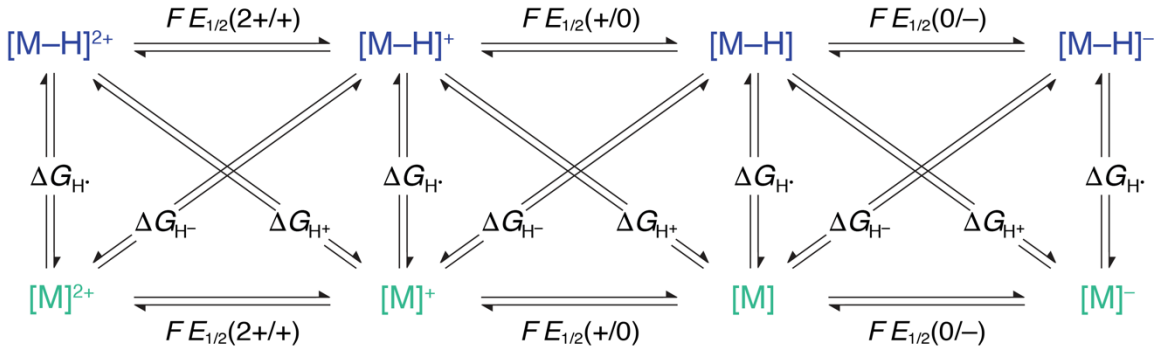

In addition to the free energy parameters depicted above, the thermodynamic constants that connect $H^\bullet$, H^+, H^- and H_2 must be adequately included to complete specific thermodynamic cycles.[8] For a complete list of these physical quantities, the authors recommend the review article in reference [2]. For this discussion, only the thermodynamic free energy required for the reactions listed below will be considered relevant.

$H^{+}_{(solv)} + e^{-} \rightleftharpoons H^{\bullet}_{(solv)}$	$\Delta G^{o}_{H^{+}/H\bullet} = 53.6$ kcal mol^{-1}	S4.1
$H^{\bullet}_{(solv)} + e^{-} \rightleftharpoons H^{-}_{(solv)}$	$\Delta G^{o}_{H\bullet/H^{-}} = 26$ kcal mol^{-1}	S4.2

Standard free energy values at 1 M H$^{\bullet}$, H^{+}, and H^{-}, referenced to the Fc$^{+/0}$ couple.

According to the diagram above, a series of mathematical representations may be written to quantify a particular thermodynamic quantity of interest, yet they all must afford self-consistent values throughout. Equation S5.4 describes the homolytic bond dissociation free energy, $\Delta G_{H\bullet}$, of a metal hydride, [M–H]$^{+}$ in terms of its hydricity value and the first reduction potential of the parent *solvent* complex, [M]$^{2+}$.

$[M-H]^{+} \rightleftharpoons [M]^{2+} + H^{-}$	$\Delta G_{H^{-}}$	(–39)[a]	(–51)[b]	S5.1
$[M]^{2+} + e^{-} \rightleftharpoons [M]^{+}$	$-nFE_{1/2}(M^{2+/+})\,; n = 1$	(23.06 × 1.68)[a]	(23.06 × 1.66)[b]	S5.2
$H^{-} \rightleftharpoons H^{\bullet} + e^{-}$	$-\Delta G_{H\bullet/H^{-}}$	(–26)[a]	(–26)[b]	S5.3
$[M-H]^{+} \rightleftharpoons [M]^{+} + H^{\bullet}$	$\Delta G_{H\bullet} = \Delta G_{H^{-}} - FE_{1/2}(M^{2+/+}) - \Delta G_{H\bullet/H^{-}}$			S5.4

[a]Calculation for [Ru(tpy)(bpy)(H)]$^{+}$. [b]Calculation for [Ru(dmb)$_2$(CO)(H)]$^{+}$. Values are given in kcal/mol^{-1}.

Direct application of Equation S5.4 provided $\Delta G_{H\bullet}$ = 52 kcal mol^{-1} for [Ru(tpy)(bpy)(H)]$^{+}$ and $\Delta G_{H\bullet}$ = 63 kcal mol^{-1} for [Ru(dmb)$_2$(CO)(H)]$^{+}$.

The free energy for proton dissociation of a metal hydride, $\Delta G_{H^{+}}$, was determined by combining $\Delta G_{H\bullet}$ and the second reduction of the parent *solvento* complex according to the set of equations S6.1–S6.4.

$[M-H]^{+} \rightleftharpoons [M]^{+} + H^{\bullet}$	$\Delta G_{H\bullet}$	(51.7)[a]	(63.3)[b]	S6.1
$[M]^{+} + e^{-} \rightleftharpoons [M]^{0}$	$-nFE_{1/2}(M^{+/0})\,; n = 1$	(23.06 × 1.98)[a]	(23.06 × 1.86)[b]	S6.2
$H^{\bullet} \rightleftharpoons H^{+} + e^{-}$	$-\Delta G_{H^{+}/H\bullet}$	(–53.6)[a]	(–53.6)[b]	S6.3
$[M-H]^{+} \rightleftharpoons [M]^{0} + H^{+}$	$\Delta G_{H^{+}} = \Delta G_{H\bullet} - FE_{1/2}(M^{+/0}) - \Delta G_{H^{+}/H\bullet}$			S6.4

[a]Calculation for [Ru(tpy)(bpy)(H)]$^{+}$. [b]Calculation for [Ru(dmb)$_2$(CO)(H)]$^{+}$. Values are given in kcal/mol^{-1}.

Direct application of equation S6.4 gave $\Delta G_{H^{+}}$ = 53 kcal mol^{-1} for [Ru(dmb)$_2$(CO)(H)]$^{+}$. With the free energy for proton dissociation being related to the acidity of a metal-hydride bond through $\Delta G_{H^{+}} = 1.364 \times pK_a$,[8] [Ru(dmb)$_2$(CO)(H)]$^{+}$ has pK_a = 39. The methodology described above was also applied to [Ru(tpy)(bpy)(H)]$^{+}$, from which $\Delta G_{H^{+}}$ = 43 kcal mol^{-1} and pK_a = 32 were obtained. The hydricity value and reduction potentials for [Ru(tpy)(bpy)(H)]$^{+}$ were available from reference **[6].**[5]

The homolytic cleavage of the metal hydride bond for the singly-reduced complexes was calculated using the thermochemical cycle described by the set of equations S7.1–S7.4, which relate the acidity of the resting state of the metal hydride with its first reduction potential.

$[\mathrm{M-H}]^{+} \rightleftharpoons [\mathrm{M}]^{0} + \mathrm{H}^{+}$	ΔG_{H^+}	(43.8)[a]	(52.6)[b]	S7.1
$[\mathrm{M-H}]^{0} \rightleftharpoons [\mathrm{M-H}]^{+} + \mathrm{e}^{-}$	$nFE_{1/2}(\mathrm{M}^{+/0})\,; n = 1$	(–23.06 × 1.98)[a]	(–23.06 × 1.93)[b]	S7.2
$\mathrm{H}^{+} + \mathrm{e}^{-} \rightleftharpoons \mathrm{H}^{\bullet}$	$\Delta G_{\mathrm{H}^+/\mathrm{H}\bullet}$	(53.6)[a]	(53.6)[b]	S7.3
$[\mathrm{M-H}]^{0} \rightleftharpoons [\mathrm{M}]^{0} + \mathrm{H}^{\bullet}$	$\Delta G_{\mathrm{H}\bullet} = \Delta G_{\mathrm{H}^-} - FE_{1/2}(\mathrm{M}^{+/0}) - \Delta \mathrm{G}_{\mathrm{H}\bullet/\mathrm{H}^-}$			S7.4

[a]Calculation for [Ru(tpy)(bpy)(H)]^0. [b]Calculation for [Ru(dmb)$_2$(CO)(H)]^0. Values are given in kcal/mol^{-1}.

The obtained values were, $\Delta G_{H\bullet}$ = 52 kcal mol^{-1} for [Ru(tpy)(bpy)(H)]^0 and $\Delta G_{H\bullet}$ = 62 kcal mol^{-1} for [Ru(dmb)$_2$(CO)(H)]^0.

The hydricity of singly-reduced [Ru(dmb)$_2$(CO)(H)]^0 was determined according to the set of equations S8.1–S8.4, which relate the $\Delta G_{\mathrm{H}\bullet}$ of the singly-reduced metal hydride with the second reduction potential of the parent *solvento* complex,

$[\mathrm{M-H}]^{0} \rightleftharpoons [\mathrm{M}]^{0} + \mathrm{H}^{\bullet}$	$\Delta G_{\mathrm{H}\bullet}$	(51.7)[a]	(61.7)[b]	S8.1
$[\mathrm{M}]^{0} \rightleftharpoons [\mathrm{M}]^{+} + \mathrm{e}^{-}$	$nFE_{1/2}(\mathrm{M}^{+/0})\,; n = 1$	(–23.06 × 2.23)[a]	(–23.06 × 2.13)[b]	S8.2
$\mathrm{H}^{\bullet} + \mathrm{e}^{-} \rightleftharpoons \mathrm{H}^{-}$	$\Delta G_{\mathrm{H}\bullet/\mathrm{H}^-}$	(26)[a]	(26)[b]	S8.3
$[\mathrm{M-H}]^{0} \rightleftharpoons [\mathrm{M}]^{+} + \mathrm{H}^{-}$	$\Delta G_{\mathrm{H}^-} = \Delta G_{\mathrm{H}\bullet} + FE_{1/2}(\mathrm{M}^{+/0}) + \Delta \mathrm{G}_{\mathrm{H}\bullet/\mathrm{H}^-}$			S8.4

[a]Calculation for [Ru(tpy)(bpy)(H)]^0. [b]Calculation for [Ru(dmb)$_2$(CO)(H)]^0. Values are given in kcal/mol^{-1}.

which provided ΔG_{H^-} = 32 kcal mol^{-1} for [Ru(tpy)(bpy)(H)]^0 and ΔG_{H^-} = 45 kcal mol^{-1} for [Ru(dmb)$_2$(CO)(H)]^0. The calculated ΔG_{H^-} values for two different redox states of the same metal hydride show that ligand-based reductions inductively increase the electron density at the metal-hydride bond, which is translated to lower hydricity values – or better hydride donors – while the homolytic cleavage to yield a H$^{\bullet}$–atom is little affected. This observation is in accordance with the fact that reported hydricities for metal hydrides span a wide range of more than 50 kcal mol^{-1},[8, 13] while $\Delta G_{\mathrm{H}\bullet}$ typically varies within a narrower range of 20 kcal mol^{-1}.[14-17]

The acidity of singly-reduced metal hydrides is usually challenging to obtain using thermochemical cycles, as it requires a knowledge of the third reduction of the *solvento* complex, according to the set of equations S9.1–S9.4.

$[M-H]^0 \rightleftharpoons [M]^0 + H^\bullet$	$\Delta G_{H^\bullet}$	(51.7)[a]	(61.7)[b]	S9.1
$[M]^0 + e^- \rightleftharpoons [M]^-$	$-nFE_{1/2}(M^{0/-}); n = 1$	(23.06 × 2.33)[a]	(23.06 × 2.18)[b]	S9.2
$H^\bullet \rightleftharpoons H^+ + e^-$	$-\Delta G_{H^+/H^\bullet}$	(–53.6)[a]	(–53.6)[b]	S9.3
$[M-H]^0 \rightleftharpoons [M]^- + H^+$	$\Delta G_{H^+} = \Delta G_{H^\bullet} - FE_{1/2}(M^{0/-}) - \Delta G_{H^+/H^\bullet}$			S9.4

[a]Calculation for $[Ru(tpy)(bpy)(H)]^0$. [b]Calculation for $[Ru(dmb)_2(CO)(H)]^0$. Values are given in kcal/mol^{-1}.

For $[Ru(tpy)(bpy)(H)]^+$, the third reduction potential of the parent $[Ru(tpy)(bpy)(CH_3CN)]^{2+}$ has been reported to occur at $E_{1/2}(M^{0/-}) = -2.33$ V vs $Fc^{+/0}$,[5] and by using equation S9.4, the acidity of $[Ru(tpy)(bpy)(H)]^0$ is pK_a = 38. For $[Ru(dmb)_2(CO)(H)]^0$ studied here, the third reduction potential of $[Ru(dmb)_2(CO)(CH_3CN)]^{2+}$ is in fact related to the one-electron reduction of the 5-corrdinate $[Ru(dmb)_2(CO)]^{0/-}$, and by using this reduction, $E_{1/2}(M^{0/-}) = -2.18$ V vs $Fc^{+/0}$, the acidity of $[Ru(dmb)_2(CO)(H)]^0$ was estimated as pK_a = 43.

The homolytic cleavage of the doubly-reduced $[M–H]^-$ was determined using the set of equations S10.1–S10.4, which relate the acidity of the singly-reduced $[M–H]^0$ with the second reduction of the metal hydride, $[M–H]^{0/-}$.

$[M-H]^0 \rightleftharpoons [M]^- + H^+$	ΔG_{H^+}	(51.9)[a]	(58.3)[b]	S10.1
$[M-H]^- \rightleftharpoons [M-H]^0 + e^-$	$nFE_{1/2}(M^{0/-}); n = 1$	(–23.06 × 2.23)[a]	(–23.06 × 2.13)[b]	S10.2
$H^+ + e^- \rightleftharpoons H^\bullet$	$\Delta G_{H^+/H^\bullet}$	(53.6)[a]	(53.6)[b]	S10.3
$[M-H]^- \rightleftharpoons [M]^- + H^\bullet$	$\Delta G_{H^\bullet} = \Delta G_{H^+} + FE_{1/2}(M^{0/-}) + \Delta G_{H^+/H^\bullet}$			S10.4

[a]Calculation for $[Ru(tpy)(bpy)(H)]^-$. [b]Calculation for $[Ru(dmb)_2(CO)(H)]^-$. Values are given in kcal/mol^{-1}.

Equation S10.4 provided $\Delta G_{H^\bullet}$ = 54 kcal mol^{-1} for $[Ru(tpy)(bpy)(H)]^-$ and $\Delta G_{H^\bullet}$ = 63 kcal mol^{-1} for $[Ru(dmb)_2(CO)(H)]^-$.

The hydricity of a doubly-reduced $[M–H]^-$ was determined by direct application of equation S11.4, which relates the free energy for the homolytic cleavage of $[M–H]^-$, $\Delta G_{H^\bullet}$, with the third reduction of the parent *solvento* complex, $[M]^{0/-}$.

$[M-H]^- \rightleftharpoons [M]^- + H^\bullet$	$\Delta G_{H^\bullet}$	(54)[a]	(62.8)[b]	S11.1
$[M]^- \rightleftharpoons [M]^0 + e^-$	$nFE_{1/2}(M^{0/-}); n = 1$	(–23.06 × 2.33)[a]	(–23.06 × 2.13)[b]	S11.2
$H^\bullet + e^- \rightleftharpoons H^-$	$\Delta G_{H^\bullet/H^-}$	(26)[a]	(26)[b]	S11.3
$[M-H]^0 \rightleftharpoons [M]^+ + H^-$	$\Delta G_{H^-} = \Delta G_{H^\bullet} + FE_{1/2}(M^{0/-}) + \Delta G_{H^\bullet/H^-}$			S11.4

[a]Calculation for $[Ru(tpy)(bpy)(H)]^-$. [b]Calculation for $[Ru(dmb)_2(CO)(H)]^-$. Values are given in kcal/mol^{-1}.

The obtained values were ΔG_{H^-} = 26 kcal mol^{-1} for [Ru(tpy)(bpy)(H)]$^-$ and ΔG_{H^-} = 39 kcal mol^{-1} for [Ru(dmb)$_2$(CO)(H)]$^-$.

Thermodynamic relationships that follow the diagram described in the beginning of this section do not allow for estimation of pK_a values for metal hydrides, as thermodynamic quantities at higher reducing states are likely inaccessible. The trend in which a metal-hydride becomes more basic (pK_a increases) as it becomes more hydridic was realized for [Ru(dmb)$_2$(CO)(H)]$^+$ and [Ru(tpy)(bpy)(H)]$^+$ and their corresponding singly-reduced forms. This was also true for [Ir(tpy)(ppy)(H)]$^+$, where ppy = 2-phenylpyridine, by using reported hydricities and reduction potentials,[12] although this analysis will not be discussed here. The question of whether the hydricity and pK_a of the doubly-reduced metal hydrides may follow a monotonic linear trend, is of interest. Shown in Scheme 3 of the main text, the solid red and blue spheres are the (ΔG_{H^-}, pK_a) xy–pairs of the resting and singly-reduced states of the listed metal hydrides. By considering that a linear trend connects the hydricities and pK_a of a metal hydride at different redox states with common $\Delta G_{\mathrm{H}^\bullet}$, the two ($\Delta G_{\mathrm{H}^-}$, p$K_a$) points for each metal hydride in Scheme 3 were used to find the equation of a *line* that connects them,

$$\Delta G_{\mathrm{H}^-} = -\left(\frac{E_{1/2}(+/0)-E_{1/2}(2+/+)}{E_{1/2}(0/-)-E_{1/2}(+/0)}\right)\Delta G_{\mathrm{H}^+} - C \qquad \text{S12}$$

where ΔG_{H^+}= 1.364 × pK_a and C is a constant. The ratio of the differences in reduction potentials in equation S12 was 0.74 for [Ru(dmb)$_2$(CO)(H)]$^+$ and 0.86 for [Ru(tpy)(bpy)(H)]$^+$. In order to generalize the utilization of equation S12, the average value (0.80) was taken, which gives,

$$\Delta G_{\mathrm{H}^-} = -1.09 \times pK_a - C \qquad \text{S13}$$

Using the known ΔG_{H^-} and pK_a values, the constant *C* was obtained for each metal hydride; *C* = 92 and 74 for Ru(CO)(H)$^{+\text{ or }0}$ and Ru(tpy)(bpy)(H)$^{+\text{ or }0}$, respectively. The final form of equation S13 is unique to each metal hydride and its displacement from the Cartesian origin in the x-direction indicates a relative measure of the homolytic bond dissociation free energy, $\Delta G_{\mathrm{H}^\bullet}$, of a metal hydride – the more distant the (ΔG_{H^-}, pK_a) trend is from the origin in the x-direction, the larger $\Delta G_{\mathrm{H}^\bullet}$ will be. By applying the known hydricities of the doubly-reduced metal hydrides, their acidities at this corresponding redox state are pK_a = 49 for Ru(CO)(H)$^-$ and pK_a = 44 for Ru(tpy)(bpy)(H)$^-$.

10. Thermodynamic relationships for the determination of the pK_a of BIH$^{\bullet+}$.

The pK_a of the radical cation, BIH$^{\bullet+}$ was determined according to the thermodynamic relationships described in the diagram below. Note that, for illustrative clarity of the diagram, the signs (*positive* or *negative*) that accompany each thermodynamic quantity for a specific reaction path were omitted.

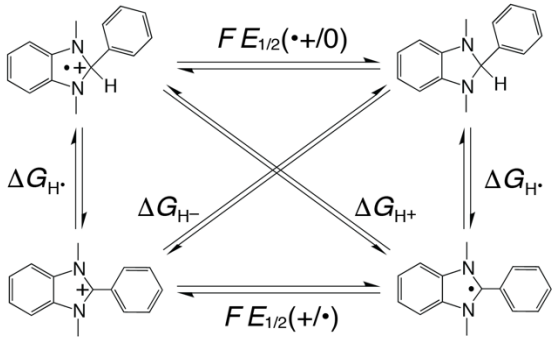

First, the homolytic bond cleavage of BIH was determined, $\Delta G_{H^\bullet}$ = 71.6 kcal mol^{-1}, according to the set of equations S14.1-S14.4. The hydricity and reduction potentials were available from references [10,11].[18-19]

$[\mathrm{BIH}] \rightleftharpoons [\mathrm{BI}^+] + \mathrm{H}^-$	ΔG_{H^-}	(50.1)	S14.1
$[\mathrm{BI}^+] + \mathrm{e}^- \rightleftharpoons [\mathrm{BI}^\bullet]$	$-nFE_{1/2}(\mathrm{BI}^{+/\bullet})\,; n = 1$	(23.06 × 2.06)	S14.2
$\mathrm{H}^- \rightleftharpoons \mathrm{H}^\bullet + \mathrm{e}^-$	$-\Delta G_{\mathrm{H}^\bullet/\mathrm{H}^-}$	(–26)	S14.3
$[\mathrm{BIH}] \rightleftharpoons [\mathrm{BI}^\bullet] + \mathrm{H}^\bullet$	$\Delta G_{\mathrm{H}^\bullet} = \Delta G_{\mathrm{H}^-} - FE_{1/2}(\mathrm{BI}^{+/\bullet}) - \Delta G_{\mathrm{H}^\bullet/\mathrm{H}^-}$		S14.4

With the obtained value for $\Delta G_{\mathrm{H}^\bullet}$, the p$K_a$ = 14.4 was calculated using the thermodynamic relationships described by the set of equations S15.1-S15.4

$[\mathrm{BIH}] \rightleftharpoons [\mathrm{BI}^\bullet] + \mathrm{H}^\bullet$	$\Delta G_{\mathrm{H}^\bullet}$	(71.6)	S15.1
$[\mathrm{BIH}^{\bullet+}] + \mathrm{e}^- \rightleftharpoons [\mathrm{BIH}]$	$-nFE_{1/2}(\mathrm{BI}^{\bullet+/0})\,; n = 1$	(23.06 × 0.07)	S15.2
$\mathrm{H}^\bullet \rightleftharpoons \mathrm{H}^+ + \mathrm{e}^-$	$-\Delta G_{\mathrm{H}^\bullet/\mathrm{H}^+}$	(–53.6)	S15.3
$[\mathrm{BIH}] \rightleftharpoons [\mathrm{BI}^+] + \mathrm{H}^-$	$\Delta G_{\mathrm{H}^+} = 1.364 \times pK_a = \Delta G_{\mathrm{H}^\bullet} - nFE_{1/2}(\mathrm{BI}^{\bullet+/0}) - \Delta G_{\mathrm{H}^\bullet/\mathrm{H}^+}$		S15.4

11. Supplementary DFT data

$[Ru(dmb)_2(CO)(CH_3CN)]^+$

Transition State for CH_3CN release

1	Ru	0.023013	-1.75E-01	-0.658256
2	N	0.611822	-4.17E-01	1.45619
3	C	1.817728	0.106791	1.765654
4	C	2.296645	0.064072	3.075052
5	H	3.263221	0.487894	3.33028
6	C	1.523474	-0.527011	4.064123
7	C	0.283761	-1.060986	3.731989
8	H	-0.351807	-1.531735	4.476371
9	C	-0.132934	-0.979718	2.411814
10	H	-1.097656	-1.379442	2.098787
11	N	1.950621	0.712604	-0.565391
12	C	2.560103	0.721479	0.651273
13	C	3.816461	1.301526	0.81956
14	H	4.294415	1.301299	1.79453
15	C	4.461918	1.88295	-0.260567
16	C	3.830644	1.876268	-1.498326
17	H	4.291294	2.318967	-2.376813
18	C	2.583207	1.284296	-1.604868
19	H	2.05977	1.25757	-2.557004
20	N	-1.913748	-1.018063	-0.357664
21	C	-2.888635	-0.162331	0.058735
22	C	-4.130314	-0.65034	0.480974
23	H	-4.884722	0.040496	0.849511
24	C	-4.374836	-2.011228	0.462101
25	C	-3.369444	-2.878219	0.024967
26	H	-3.521625	-3.95309	-0.011894
27	C	-2.158287	-2.339955	-0.367561
28	H	-1.334998	-2.965844	-0.708195
29	N	-1.205146	1.524931	0.05947
30	C	-2.540138	1.251822	0.050079
31	C	-3.489585	2.278408	0.007049
32	H	-4.549142	2.038174	-0.049956
33	C	-3.068641	3.596053	0.007648
34	C	-1.694824	3.869131	0.037872
35	H	-1.321521	4.88962	0.059258
36	C	-0.808721	2.810474	0.044423
37	H	0.269738	2.972948	0.05192
38	C	-0.267608	0.104812	-2.457864
39	O	-0.439325	0.306733	-3.596665
40	H	1.888299	-0.56675	5.087539
41	H	5.442303	2.335076	-0.134831
42	H	-5.334091	-2.399677	0.7959
43	H	-3.794345	4.40497	-0.02797
44	N	1.149092	-2.274505	-0.915474
45	C	1.896184	-3.113086	-1.206812
46	C	2.825855	-4.160631	-1.57512
47	H	3.843268	-3.759442	-1.627522
48	H	2.801223	-4.965405	-0.833186
49	H	2.557845	-4.573132	-2.553239

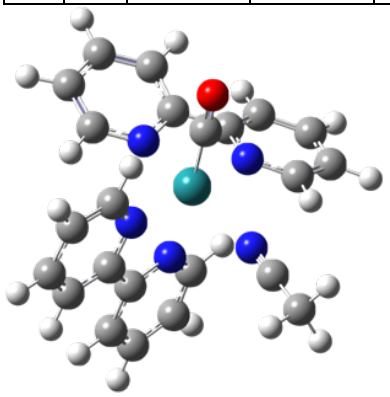

$[Ru(dmb)_2(CO)(CH_3CN)]^0$

Transition State for CH_3CN release

1	Ru	0.005232	4.08E-01	-0.866245
2	N	-0.110175	4.96E-01	1.254979
3	C	-1.402568	0.450209	1.736933
4	C	-1.630172	0.397726	3.132649
5	H	-2.649604	0.341676	3.508979
6	C	-0.575904	0.464715	4.007438
7	C	0.738528	0.588605	3.496899
8	H	1.599359	0.666537	4.15544
9	C	0.911501	0.590564	2.134078
10	H	1.907454	0.656343	1.692409
11	N	-2.005496	0.822526	-0.541951
12	C	-2.42858	0.523541	0.749723
13	C	-3.797403	0.299722	1.01172
14	H	-4.105705	0.014555	2.015826
15	C	-4.731134	0.415326	0.012413
16	C	-4.295727	0.763076	-1.287094
17	H	-4.997816	0.889144	-2.10719
18	C	-2.951758	0.93835	-1.507747
19	H	-2.578891	1.184037	-2.500981
20	N	2.038802	-0.230065	-0.675852
21	C	2.099397	-1.494161	-0.139298
22	C	3.345142	-2.026872	0.250492
23	H	3.394996	-3.028375	0.672563
24	C	4.495138	-1.293975	0.060265
25	C	4.419745	-0.031171	-0.556258
26	H	5.30622	0.572185	-0.730714
27	C	3.17392	0.443541	-0.916577
28	H	3.048571	1.422959	-1.378266
29	N	-0.196189	-1.652068	-0.765652
30	C	0.848467	-2.190279	-0.032598
31	C	0.644398	-3.372405	0.711188
32	H	1.435245	-3.739984	1.363205
33	C	-0.552071	-4.042655	0.624455
34	C	-1.576853	-3.526917	-0.204316
35	H	-2.519432	-4.051876	-0.33494
36	C	-1.366251	-2.324343	-0.835154
37	H	-2.145141	-1.849566	-1.434841
38	C	-0.040822	0.492504	-2.726521
39	O	-0.11271	0.565451	-3.890961
40	H	-0.751058	0.444943	5.081162
41	H	-5.784644	0.237326	0.216467
42	H	5.457973	-1.702073	0.361036
43	H	-0.711725	-4.956542	1.192812
44	N	0.716104	2.768573	-0.656332
45	C	1.40463	3.414248	0.023349
46	C	2.28651	4.170294	0.889387
47	H	2.47459	5.167326	0.477177
48	H	1.838005	4.277016	1.882782
49	H	3.242968	3.64417	0.990653

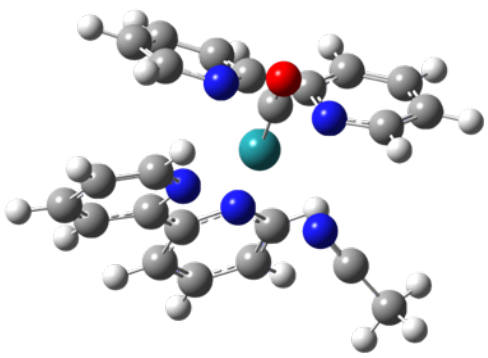

$[Ru(dmb)_2(CO)(HCOO)]^0$

Transition State for O-bound $HCOO^-$ isomer

1	Ru	0.000991	0.666708	-0.363595
2	N	-0.491278	-0.519501	1.416383
3	C	-1.761774	-0.962768	1.480059
4	C	-2.18207	-1.779619	2.528966
5	H	-3.204232	-2.143178	2.579301
6	C	-1.274287	-2.131377	3.518261
7	C	0.030251	-1.657772	3.444796
8	H	0.768396	-1.90598	4.202039
9	C	0.379371	-0.850878	2.371109
10	H	1.384001	-0.442139	2.264419
11	N	-2.074988	0.245872	-0.575619
12	C	-2.649221	-0.511376	0.393146
13	C	-4.007269	-0.820608	0.350534
14	H	-4.458089	-1.422219	1.13406
15	C	-4.787781	-0.351064	-0.694871
16	C	-4.192656	0.429023	-1.678734
17	H	-4.761561	0.823481	-2.515721
18	C	-2.838933	0.704924	-1.578716
19	H	-2.33564	1.316651	-2.32275
20	N	2.019683	0.798078	0.147707
21	C	2.772057	-0.31045	-0.212581
22	C	4.148316	-0.342999	0.13305
23	H	4.748571	-1.208222	-0.140853
24	C	4.715715	0.704268	0.811045
25	C	3.925327	1.823504	1.166564
26	H	4.340762	2.6688	1.70749
27	C	2.593522	1.816793	0.808173
28	H	1.919593	2.631914	1.066897
29	N	0.714478	-1.116028	-1.102007
30	C	2.071086	-1.337945	-0.887741
31	C	2.639054	-2.551519	-1.356507
32	H	3.700029	-2.734697	-1.199068
33	C	1.867154	-3.481579	-1.999883
34	C	0.488005	-3.227202	-2.205482
35	H	-0.157473	-3.93693	-2.714396
36	C	-0.026239	-2.03596	-1.743781
37	H	-1.076159	-1.781357	-1.885368
38	C	0.242699	1.53867	-1.962417
39	O	0.345459	2.071509	-2.993787
40	H	-1.58716	-2.76921	4.341398
41	H	-5.847555	-0.589394	-0.736663
42	H	5.771226	0.67251	1.075042
43	H	2.313032	-4.408626	-2.354801
44	O	-0.342952	2.273099	1.74159
45	C	-0.920716	3.128826	1.038496
46	O	-1.10454	3.060157	-0.198276
47	H	-1.310013	4.039039	1.554784

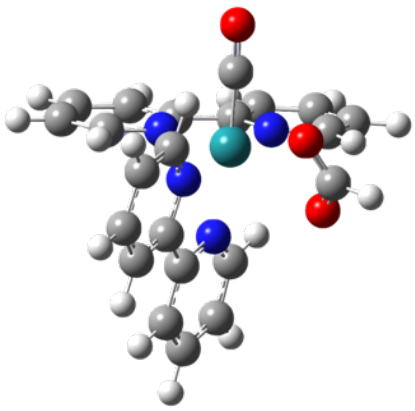

$[Ru(dmb)_2(CO)(HCOO)]^0$

Transition State for $HCOO^-$ release

1	Ru	-0.10048	0.767917	-0.17755
2	N	-0.40233	-1.00181	1.067372
3	C	-1.6359	-1.55322	0.993179
4	C	-1.92534	-2.74803	1.652812
5	H	-2.9111	-3.19798	1.578551
6	C	-0.93839	-3.37117	2.401711
7	C	0.319481	-2.78424	2.489433
8	H	1.118342	-3.23332	3.072623
9	C	0.540414	-1.59872	1.806403
10	H	1.507855	-1.09934	1.842742
11	N	-2.14308	0.291342	-0.45541
12	C	-2.61547	-0.81173	0.188164
13	C	-3.95432	-1.19105	0.091457
14	H	-4.31452	-2.06738	0.622851
15	C	-4.83079	-0.442	-0.67637
16	C	-4.34441	0.68736	-1.32823
17	H	-4.98958	1.313476	-1.93857
18	C	-3.00862	1.018285	-1.18766
19	H	-2.59788	1.902725	-1.66606
20	N	2.034447	0.943553	0.225362
21	C	2.873716	0.034506	-0.32803
22	C	4.258784	0.170567	-0.21251
23	H	4.914633	-0.55064	-0.69492
24	C	4.780861	1.242848	0.4938
25	C	3.908888	2.16335	1.072471
26	H	4.275955	3.011735	1.643423
27	C	2.545557	1.979237	0.906214
28	H	1.80798	2.654826	1.337175
29	N	1.023709	-0.86475	-1.55588
30	C	2.23504	-1.10545	-0.99977
31	C	2.803361	-2.38134	-0.97691
32	H	3.764511	-2.54178	-0.49198
33	C	2.105277	-3.44263	-1.53312
34	C	0.852322	-3.19783	-2.10084
35	H	0.272551	-3.99733	-2.55561
36	C	0.360114	-1.90344	-2.08864
37	H	-0.61295	-1.66827	-2.52349
38	C	-0.07252	2.168063	-1.37208
39	O	-0.11015	3.039268	-2.15624
40	H	-1.15219	-4.30561	2.915006
41	H	-5.87552	-0.73083	-0.75892
42	H	5.857634	1.365199	0.586688
43	H	2.520402	-4.4476	-1.51179
44	O	-0.51635	2.01041	1.774029
45	C	-1.25113	3.044458	1.704438
46	O	-1.79772	3.551975	0.720756
47	H	-1.40201	3.545309	2.700424

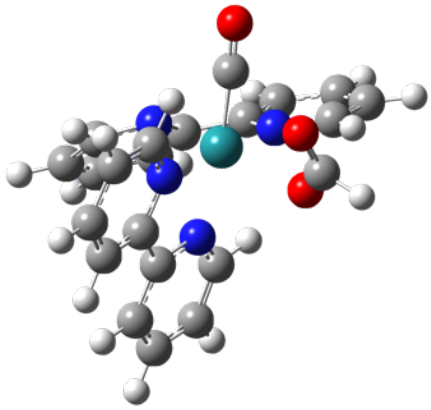

[Ru(dmb)$_2$(CO)(HCOO)]$^-$

Transition State for HCOO$^-$ release

1	Ru	-4.85E-02	0.705473	-0.310973
2	N	-1.66E-01	-0.573882	1.378928
3	C	-1.377444	-1.2273	1.499604
4	C	-1.546172	-2.22841	2.486105
5	H	-2.500025	-2.745685	2.567832
6	C	-0.526106	-2.526281	3.352065
7	C	0.696318	-1.8196	3.243937
8	H	1.525724	-2.012777	3.919228
9	C	0.821331	-0.87686	2.25435
10	H	1.749837	-0.319681	2.122188
11	N	-2.079097	0.33184	-0.158632
12	C	-2.401494	-0.777133	0.616328
13	C	-3.672045	-1.381138	0.498628
14	H	-3.894128	-2.268849	1.08797
15	C	-4.615614	-0.872369	-0.358159
16	C	-4.288009	0.270924	-1.122839
17	H	-5.004925	0.723618	-1.803299
18	C	-3.035263	0.815935	-0.994905
19	H	-2.746791	1.69205	-1.573635
20	N	2.083259	0.688691	-0.170823
21	C	2.607049	-0.523447	-0.527659
22	C	3.977496	-0.778308	-0.343019
23	H	4.393885	-1.740599	-0.633376
24	C	4.791008	0.209808	0.172688
25	C	4.244148	1.464079	0.484189
26	H	4.855477	2.262464	0.896405
27	C	2.888619	1.65894	0.28719
28	H	2.372374	2.580889	0.557889
29	N	0.479783	-0.93376	-1.529108
30	C	1.668108	-1.471211	-1.081336
31	C	1.907834	-2.854378	-1.186279
32	H	2.804812	-3.281865	-0.740688
33	C	0.99691	-3.660858	-1.831175
34	C	-0.17515	-3.083237	-2.364607
35	H	-0.899523	-3.677617	-2.915696
36	C	-0.401187	-1.741799	-2.155893
37	H	-1.321577	-1.259267	-2.490748
38	C	-0.156731	2.00663	-1.63438
39	O	-0.272575	2.862322	-2.427186
40	H	-0.659754	-3.285373	4.120188
41	H	-5.593048	-1.34122	-0.448215
42	H	5.85255	0.020141	0.319237
43	H	1.174708	-4.730504	-1.919911
44	O	0.258671	2.980536	1.258381
45	C	-0.491389	3.989105	1.172661
46	O	-1.698689	4.060067	0.890894
47	H	0.027212	4.971284	1.393199

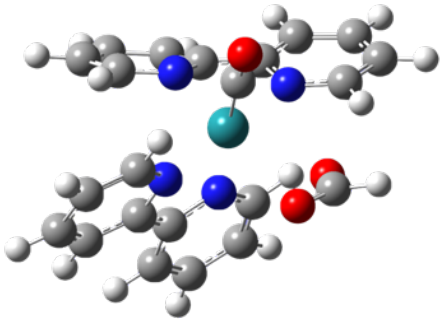

$[Ru(dmb)_2(CO)(H)]^0$
Transition State for Hydride Transfer to CO_2
Hydride Abstraction Step

1	Ru	-0.027319	-0.124491	-0.796043
2	H	0.49857	-1.685511	-1.403938
3	N	0.542931	-0.684356	1.232758
4	C	1.812325	-0.372318	1.573253
5	C	2.291859	-0.643583	2.852896
6	H	3.311547	-0.394663	3.130797
7	C	1.451148	-1.242639	3.781161
8	C	0.149403	-1.561947	3.415659
9	H	-0.537953	-2.033451	4.11193
10	C	-0.264767	-1.264399	2.125547
11	H	-1.271787	-1.495279	1.77904
12	N	2.012225	0.446748	-0.679986
13	C	2.627731	0.246782	0.513439
14	C	3.959107	0.608792	0.702745
15	H	4.440966	0.447525	1.662378
16	C	4.674574	1.176715	-0.340845
17	C	4.03964	1.371007	-1.56081
18	H	4.55601	1.809523	-2.409751
19	C	2.712467	0.993334	-1.685901
20	H	2.178889	1.132005	-2.622909
21	N	-2.014884	-0.677879	-0.479371
22	C	-2.807741	0.310246	0.092803
23	C	-4.167871	0.012288	0.369994
24	H	-4.800699	0.776011	0.817207
25	C	-4.682863	-1.224379	0.083057
26	C	-3.851055	-2.214442	-0.495385
27	H	-4.221637	-3.208039	-0.730382
28	C	-2.538587	-1.885661	-0.756556
29	H	-1.839453	-2.60724	-1.179682
30	N	-0.830143	1.644238	0.042654
31	C	-2.174757	1.548918	0.37055
32	C	-2.814867	2.678127	0.947263
33	H	-3.871236	2.621781	1.201625
34	C	-2.11327	3.831	1.182795
35	C	-0.739801	3.899128	0.844704
36	H	-0.149661	4.794606	1.016301
37	C	-0.161364	2.783451	0.277702
38	H	0.88975	2.782224	-0.013599
39	C	-0.335736	0.372136	-2.544689
40	O	-0.498419	0.69305	-3.653081
41	H	1.814348	-1.458759	4.782899
42	H	5.714046	1.461757	-0.200451
43	H	-5.726718	-1.442798	0.300747
44	H	-2.612642	4.690735	1.625694
45	C	1.0913	-2.855036	-0.937351
46	O	2.28832	-2.714802	-0.976169
47	O	0.19979	-3.630646	-0.686575

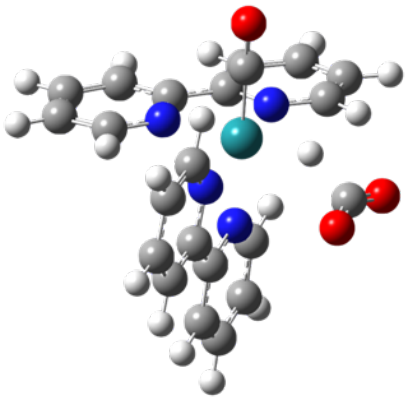

$[Ru(dmb)_2(CO)(H)]^0$
Transition State for Hydride Transfer to CO_2
Rotational Rearrangement Step

1	Ru	0.098588	0.061841	-0.571059
2	H	1.170424	-1.881526	-3.080511
3	N	0.646567	-0.574706	1.450521
4	C	1.924249	-0.301244	1.794738
5	C	2.425947	-0.686238	3.038529
6	H	3.449483	-0.457734	3.320677
7	C	1.602326	-1.362932	3.925841
8	C	0.289585	-1.63975	3.559613
9	H	-0.388788	-2.165845	4.225185
10	C	-0.144346	-1.224579	2.31012
11	H	-1.163919	-1.414798	1.975513
12	N	2.043808	0.824712	-0.326712
13	C	2.711915	0.432046	0.793794
14	C	4.062949	0.72564	0.970204
15	H	4.58161	0.392681	1.864635
16	C	4.751102	1.435517	-0.000817
17	C	4.062524	1.84279	-1.138192
18	H	4.551483	2.403088	-1.930304
19	C	2.723711	1.515895	-1.260915
20	H	2.158299	1.810651	-2.141025
21	N	-1.780059	-1.012453	-0.561724
22	C	-2.929812	-0.453894	-0.120898
23	C	-4.093747	-1.21296	-0.001885
24	H	-5.001615	-0.761901	0.390024
25	C	-4.076167	-2.554278	-0.356703
26	C	-2.889839	-3.11538	-0.815671
27	H	-2.82983	-4.162151	-1.10061
28	C	-1.762495	-2.312013	-0.898649
29	H	-0.78627	-2.680875	-1.2217
30	N	-1.658214	1.468997	0.520486
31	C	-2.87855	0.975884	0.247744
32	C	-4.021773	1.774725	0.29754
33	H	-4.996638	1.369399	0.037632
34	C	-3.892698	3.1104	0.655935
35	C	-2.630191	3.613791	0.950174
36	H	-2.486169	4.651955	1.237724
37	C	-1.542736	2.752947	0.860569
38	H	-0.530094	3.101135	1.069432
39	C	-0.178934	0.772367	-2.249761
40	O	-0.315158	1.258981	-3.309291
41	H	1.983331	-1.668075	4.897527
42	H	5.805487	1.665583	0.129203
43	H	-4.977541	-3.155744	-0.264813
44	H	-4.769706	3.752415	0.695983
45	C	1.883043	-1.934722	-2.2024
46	O	3.089734	-1.812618	-2.447572
47	O	1.31936	-2.120012	-1.081819

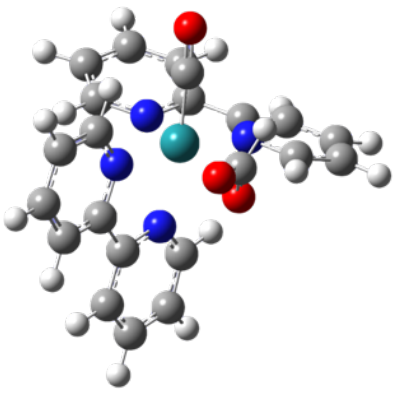

References

(1) Pavlishchuk, V.; Addison, A. W., Conversion Constants for Redox Potentials Measured Versus Different Reference Electrodes in Acetonitrile Solutions at 25°C. *Inorg. Chim. Acta.* 2000, *298*, 97-102.
(2) Fujita, E.; Creutz, C.; Sutin, N.; Szalda, D. J., Carbon dioxide activation by cobalt(I) macrocycles: factors affecting carbon dioxide and carbon monoxide binding. *J. Am. Chem. Soc.* 1991, *113*, 343-353.
(3) Furenlid, L. R.; Renner, M. W.; Szalda, D. J.; Fujita, E., EXAFS Studies of Nickel(II), Nickel(I), and Ni(I)-CO Tetraazamacrocycles and the Crystal Structure of (5,7,7,12,14,14-Hexamethyl-1,4,8,11-Tetraazacyclotetradeca-4,11-diene)nickel(I) Perchlorate. *J. Am. Chem. Soc.* 1991, *113*, 883-892.
(4) Hayashi, Y.; Kita, S.; Brunschwig, B. S.; Fujita, E., Involvement of a Binuclear Species with the Re−C(O)O−Re Moiety in CO_2 Reduction Catalyzed by Tricarbonyl Rhenium(I) Complexes with Diimine Ligands: Strikingly Slow Formation of the Re−Re and Re−C(O)O−Re Species from $Re(dmb)(CO)_3S$ (dmb = 4,4‘-Dimethyl-2,2‘-bipyridine, S = Solvent). *J. Am. Chem. Soc.* 2003, *125*, 11976-11987.
(5) Matsubara, Y.; Fujita, E.; Doherty, M. D.; Muckerman, J. T.; Creutz, C., Thermodynamic and Kinetic Hydricity of Ruthenium(II) Hydride Complexes. *J. Am. Chem. Soc.* 2012, *134*, 15743-15757.
(6) Fujita, E.; Creutz, C.; Sutin, N.; Brunschwig, B. S., Carbon Dioxide Activation by Cobalt Macrocycles: Evidence of Hydrogen Bonding Between Bound CO_2 and the Macrocycle in Solution. *Inorg. Chem.* 1993, *32*, 2657-2662.
(7) Matsubara, Y.; Hightower, S. E.; Chen, J.; Grills, D. C.; Polyansky, D. E.; Muckerman, J. T.; Tanaka, K.; Fujita, E., Reactivity of a fac-$ReCl(\alpha\text{-diimine})(CO)_3$ Complex With an NAD^+ Model Ligand Toward CO_2 Reduction. *Chem. Commun.* 2014, *50*, 728-730.
(8) Wiedner, E. S.; Chambers, M. B.; Pitman, C. L.; Bullock, R. M.; Miller, A. J. M.; Appel, A. M., Thermodynamic Hydricity of Transition Metal Hydrides. *Chem. Rev.* 2016, *116*, 8655-8692.
(9) Hu, Y.; Norton, J. R., Kinetics and Thermodynamics of $H^-/H^\bullet/H^+$ Transfer from a Rhodium(III) Hydride. *J. Am. Chem. Soc.* 2014, *136*, 5938-5948.
(10) Izutsu, K.; Nakamura, T.; Takizawa, K.; Takeda, A., Calorimetric Determination of Thermodynamic Parameters for the Dissociations of Acids in Dipolar Aprotic Solvents. *Bull. Chem. Soc., Jpn.* 1985, *58*, 455-458.
(11) Kaljurand, I.; Kütt, A.; Sooväli, L.; Rodima, T.; Mäemets, V.; Leito, I.; Koppel, I. A., Extension of the Self-Consistent Spectrophotometric Basicity Scale in Acetonitrile to a Full Span of 28 pKa Units: Unification of Different Basicity Scales. *J. Org. Chem.* 2005, *70*, 1019-1028.
(12) Garg, K.; Matsubara, Y.; Ertem, M. Z.; Lewandowska-Andralojc, A.; Sato, S.; Szalda, D. J.; Muckerman, J. T.; Fujita, E., Striking Differences in Properties of Geometric Isomers of $[Ir(tpy)(ppy)H]^+$: Experimental and Computational Studies of their Hydricities, Interaction with CO_2, and Photochemistry. *Angew. Chem. Int. Ed.* 2015, *54*, 14128-14132.
(13) Waldie, K. M.; Ostericher, A. L.; Reineke, M. H.; Sasayama, A. F.; Kubiak, C. P., Hydricity of Transition-Metal Hydrides: Thermodynamic Considerations for CO_2 Reduction. *ACS Catal.* 2018, *8*, 1313-1324.
(14) Wayner, D. D. M.; Parker, V. D., Bond Energies in Solution from Electrode Potentials and Thermochemical Cycles. A Simplified and General Approach. *Acc. Chem. Res.* 1993, *26*, 287-294.

(15) Elkind, J. L.; Armentrout, P. B., Transition-Metal Hydride Bond Energies: First and Second Row. *Inorg. Chem.* 1986, *25*, 1078-1080.
(16) Wang, D.; Angelici, R. J., Metal−Hydrogen Bond Dissociation Enthalpies in Series of Complexes of Eight Different Transition Metals. *J. Am. Chem. Soc.* 1996, *118*, 935-942.
(17) Tilset, M., The Thermodynamics of Organometallic Systems Involving Electron-Transfer Paths. In *Electron Transfer in Chemistry*, Balzani, V., Ed. Wiley-VCH: Weinheim, Germany, 2008; Vol. II, pp 677-713.
(18) Zhu, X.-Q.; Zhang, M.-T.; Yu, A.; Wang, C.-H.; Cheng, J.-P., Hydride, Hydrogen Atom, Proton, and Electron Transfer Driving Forces of Various Five-Membered Heterocyclic Organic Hydrides and Their Reaction Intermediates in Acetonitrile. *J. Am. Chem. Soc.* 2008, *130*, 2501-2516.
(19) Ilic, S.; Pandey Kadel, U.; Basdogan, Y.; Keith, J. A.; Glusac, K. D., Thermodynamic Hydricities of Biomimetic Organic Hydride Donors. *J. Am. Chem. Soc.* 2018, *140*, 4569-4579.